Oxford Open Materials Science, 2025, **5(1)**, itaf008
https://doi.org/10.1093/oxfmat/itaf008
Advance Access Publication Date: 28 April 2025
Research article

Slurry erosion performance of WC-Co and Cr_3C_2-NiCr coatings on hydro turbine steel: optimization and modelling under variable operational conditions

Sukhinderpal Singh[1,2], Harnam Singh Farwaha[1], Raman Kumar [1,3], I. A. Ariffin[4], N. Beemkumar[5], Jasmaninder Singh Grewal[1], Inderdeep Singh[1,6], A. Bhowmik[7,8], Wulfran Fendzi Mbasso[9,10,11,*]

[1]Department of Mechanical and Production Engineering, Guru Nanak Dev Engineering College, Ludhiana, Punjab 141006, India
[2]Centre for Research Impact & Outcome, Chitkara University Institute of Engineering and Technology, Chitkara University, Rajpura, Punjab 140401, India
[3]Jadara Research Center, Jadara University, Irbid 21110, Jordan
[4]Management and Science University, Shah Alam, Selangor, Malaysia
[5]Department of Mechanical Engineering, School of Engineering and Technology, JAIN (Deemed to be University), Bangalore, Karnataka 562112, India
[6]Department of Mechanical Engineering, Chandigarh University, Gharuan, Mohali, Punjab 140413, India
[7]Department of Mechanical Engineering, Graphic Era (Deemed to be University), Clement Town, Dehradun 248002, India
[8]Division of Research and Development, Lovely Professional University, Phagwara, 144411, Punjab, India
[9]Laboratory of Technology and Applied Sciences, University Institute of Technology, University of Douala, PO Box 8698, Douala, Cameroon
[10]Department of Biosciences, Saveetha School of Engineering, Saveetha Institute of Medical and Technical Sciences, Chennai, Chennai 602 105, India
[11]Applied Science Research Center, Applied Science Private University, Amman, Jordan

*Corresponding author: Laboratory of Technology and Applied Sciences, University Institute of Technology, University of Douala, PO Box 8698, Douala, Cameroon. E-mail: fendzi.wulfran@yahoo.fr

Abstract

The effectiveness of coated and uncoated hydro-turbine steel at different slurry concentrations and impingement angles is being studied in the current effort to understand better the central problem of erosion of turbines and its components in hydropower generating plants. The pressure and stand-off distance were maintained at the same levels throughout the slurry erosion experiment. The tester for slurry erosion is additionally employed for experimental purposes. The maximum erosion occurred at a 20 000 ppm (parts per million) slurry concentration and a 30° impingement angle. While Tungsten Carbide-Cobalt (WC-Co) shows a brittle nature, Chromium Carbide-Nickel Chromium (Cr_3C_2-NiCr) exhibited brittle and ductile characteristics. While Cr_3C_2-NiCr is less resistant to slurry erosion than WC-Co, it still outperforms uncoated material. The degree of resistance to slurry erosion throughout both impact angles: Cr_3C_2-NiCr coating is superior to WC-Co coating. Statistical analyses were employed to analyze the data and identify key factors influencing erosion. Regression analysis reveals negative correlations between erosion rates and slurry concentration/impingement angle in WC-Co coated specimens, suggesting reduced erosion with decreasing concentration and angle. Analysis of Variance (ANOVA) results confirm the significant impacts of specimen type, slurry concentration, and impingement angle on erosion variability. Visual examination, X-ray Diffraction (XRD) patterns, Scanning Electron Microscopy (SEM)/Energy Dispersive X-ray Analysis (EDAX) micrographs, and elemental analysis further characterize the erosion mechanisms and coating performance, highlighting the protective effects of coatings in reducing erosion rates. This research improves erosion knowledge, optimizes performance, and directs material selection for erosion-prone situations, aiding industries facing wear and erosion concerns and enhancing component longevity and dependability.

Keywords: slurry erosion; Cr_3C_2-NiCr; WC-Co; coating; resistance

Introduction

The erosion of turbines and their components in hydropower-generating plants is a significant problem in all countries. This problem primarily affects the power facilities in India that are close to the Himalayan region [1]. Common turbine parts and other machinery impacted by slurry erosion include seat valves, top and bottom ring liners, draft tubes, runners, guiding vanes, runner blades, pipes, nozzles, and pumps. Therefore, erosion wear poses a significant risk to engineers, designers, and people operating hydropower-producing units' gear and equipment [2]. Slurry is a liquid that contains very minute solid particles such as coal, silt, sand, cement, gravel, clay, etc. Solid abrasive found in water is used in the slurry erosion to dissolve and disintegrate the substance [3]. The erosive wear rate of a material is influenced by several elements, such as its slurry concentration, erodent hardness, size, shape, and velocity [4]. The angle of incidence is a crucial element that holds significant importance. The maximum wear of ductile materials happens at 30° [5]. Nevertheless, non-ductile material at an angle normal to the target surface is considered for maximal wear [6].

Furthermore, erosion issues are common in hydro turbines, and conventional steels used in power plants such as carbon steel, white cast iron, stainless steel, low manganese steel, and many others- cannot resist them [7]. This results in significant

Received: 22 January 2025. **Revised:** 23 April 2025. **Accepted:** 23 April 2025

downtime, increased maintenance needs, and losses in revenue [8, 9]. Any covering applied to an object's or material's surface is called a coating. These are occasionally used to improve and alter the surface characteristics of substrates, giving them resistance to erosion and corrosion [10, 11]. It may also be defined as a material typically made of the same or a different material and deposited on the substrate naturally or intentionally. Coatings can be deposited in various ways, typically ranging from a few to hundreds of microns [12]. The environment in which the component must function will determine the coating's thickness, type and depositional method [13]. Therefore, it has been determined that applying different coatings can cost-effectively increase the target material's hardness and resistance to erosion [14, 15]. There are numerous methods for applying coatings. The most effective way to protect the material from corrosive and erosive wear was thermal spray coating, which involves injecting powdered material at a very high temperature to heat it up and accelerate it even faster quickly [16].

Goyal *et al.* [17] studied the slurry erosion resistance of a Cr3C2-NiCr coating applied via High Velocity Oxy-Fuel (HVOF) spray to CA6NM turbine steel. A high-speed erosion test apparatus was employed to vary parameters such as slurry particle size, speed, and concentration. Three different HVOF-sprayed cermet coatings were tested by Reyes-Mojena [18] for slurry erosion behavior. They were created using powders that included fine WC grain, Cr3C2-NiCr (75-25), and standard grain sizes of NiCrWSiFeB. Sharma *et al.* [19] investigated the slurry erosion resistance of high-velocity flame-sprayed (HVFS) nickel matrix coatings, including TiO_2 and Al_2O_3 ceramic particles. Kumar *et al.* [20] reviewed the slurry erosion effect of HVOF-sprayed coatings on hydroturbine steel. Kumar *et al.* [21] studied the slurry erosion behavior of Cr3C2-25NiCr ceramic nanocomposite coatings enhanced with nano-yttria-stabilized zirconia (YSZ) on turbine steel. Using high-velocity oxy-fuel coating, coatings containing 90% (Cr3C2-25NiCr) + 10% YSZ and 95% (Cr3C2-25NiCr) + 5% YSZ were applied. Kumar *et al.* [22] examined the erosion resistance of HVOF-sprayed Al_2O_3/Cr_2O_3 composite coatings on stainless steel (SS-304) in silt slurry conditions. Sahni and Grewal [23] used HVOF thermal spray to put a protective WC-Co-Cr coating on Cast Austenitic Stainless Steel Grade CF8M steel in turbines, extending its lifespan. Wear experiments on slurry erosion were performed with various parameters. Maekai *et al.* [24] applied WC-10Co-4Cr and Cr3C2-25(Ni20Cr) coatings to F6NM stainless steel from the Dul-Hasti hydropower facility via the HVOF technique. High-speed slurry erosive wear tests were performed on sediments from the plant dam. Babu *et al.* [25] systematically tested Ni-SiC composite claddings on SS 316 l for slurry erosion rates at different impact angles. These claddings, which were created by microwave hybrid heating, comprised 5 wt.% SiC particles of various sizes (nano to micro), either alone (unimodal) or together (bimodal) in the matrix. Paredes, *et al.* [26] investigated enhancing agricultural harvester blade performance using arc-sprayed iron-based WC coatings. Flame remelting improved adhesion, increasing impact wear resistance and blade longevity. Khuengpukheiw *et al.* [27] studied HVOF-sprayed coatings on rice harvester blades, analyzing volume loss, hardness, and surface roughness. WC-Co coatings showed superior hardness, while NiSiCrFeB had the highest volume loss. Marques *et al.* [28] investigated wear in hot forging tools, using HVOF coatings for the first time on punches. WC-CoCr exhibited lower roughness, higher hardness, and improved wear resistance compared to Cr3C2-NiCr, confirming HVOF as a promising method for extending tool life.

Kumar, *et al.* [29] studied erosion resistance in nano YSZ-reinforced WC-10Co-4Cr coatings on CA6NM steel using HVOF spraying. Nanocomposite coatings exhibited higher microhardness, lower porosity, and greater erosion resistance than conventional coatings, with 5–10% YSZ reinforcement offering the best performance. Ma and Ruggerio [30] investigated Cr_3C_2-NiCr coatings sprayed via HVOF, analyzing feedstock characteristics and sliding wear performance. The study evaluated the mechanical properties and slurry erosion behavior of $10TiO_2$-Cr_2O_3 coated turbine steel. Slurry erosion tests demonstrated the superior erosion resistance of $10TiO_2$-Cr_2O_3 coatings compared to Al_2O_3 and uncoated steel, with surface analysis revealing key erosion mechanisms [31].

As a result, thermally sprayed coatings find extensive use in various sectors [32]. It has been discovered that thermal spraying techniques are adaptable to building erosion and corrosion resistance [33, 34]. As a result, it improves the performance and working life of materials often subjected to erosive wear conditions [35]. The coating material's qualities and the spraying process's settings affect how well-deposited coatings are via the thermal spray method [36]. Union Carbide Corporation created and received a patent for the detonation spray coating apparatus in the US in 1995 [37].

In hydro turbines, slurry erosion primarily results from the high-speed impact of solid particles, such as sand, silt, and gravel, carried in the water. These particles impact turbine parts from various angles, resulting in material loss through cutting, plowing, and fatigue [38]. The severity of erosion is significantly affected by slurry concentration, as well as the size, shape, impact velocity, and angle of the particles. Ductile materials typically experience greater wear at oblique angles (around 30°), whereas brittle materials are more vulnerable during normal impacts (approximately 90°). This ongoing erosion deteriorates surface integrity, modifies blade shapes, reduces hydraulic efficiency, and may lead to rotor imbalance and vibrations [39]. Ultimately, these consequences hinder the performance, reliability, and lifespan of hydro turbine components, resulting in higher maintenance expenses and increased operational downtime. Thus, understanding and addressing slurry erosion is crucial for sustainable and cost-efficient hydropower production. Erosion of hydro-turbine components, compounded by slurry erosion, presents significant challenges to power generation. Coatings have emerged as a viable alternative for increasing erosion resistance and extending the life of turbine parts. Various coating processes provide the potential for surface modification and excellent erosion control. However, the optimal choice of coating materials, deposition techniques, and parameters remains an important research topic.

Furthermore, the interplay of slurry properties (particle size, concentration) and operational factors (impingement angle, velocity) in erosion processes necessitates further research. Understanding how these elements affect erosive wear rates and processes is crucial for designing customized coating solutions and operational methods to mitigate erosion-related challenges in hydro-turbines. Enhancing slurry erosion resistance is crucial for prolonging the lifespan of critical components in hydroelectric turbines that are subjected to abrasive conditions. Instead of just assessing erosion rates, this research focuses on identifying parameter combinations that minimize erosion through the use of statistical and experimental optimization. This method supports better decision-making in selecting materials and planning maintenance. The primary goal of this study is to evaluate and compare the slurry erosion performance of uncoated hydro turbine steel to steel coated with WC + Co and Cr3C2 + NiCr coatings. The emphasis is on overcoming erosion difficulties in biomedical and engineering settings, where erosion resistance is crucial for maintaining performance, reliability, and safety. Specifically, the study aims to:

- Evaluate the erosion resistance of uncoated hydro turbine steel under varying slurry concentrations and impingement angles representative of real-world operational conditions.
- Investigate the effectiveness of WC + Co and Cr3C2 + NiCr coatings in reducing erosion rates and enhancing durability compared to uncoated steel.
- Analyze the impact of slurry composition, particle size, velocity, and impingement angle on erosion behavior to understand the underlying mechanisms influencing erosion resistance.
- Investigate the applicability of thermal-sprayed coatings in mitigating erosion challenges across biomedical and engineering applications, taking into account factors such as coating thickness, deposition process, and material properties.
- Provide insights and recommendations for optimizing erosion performance and selecting suitable coatings for hydro-turbine steel.

This study distinguishes itself from earlier research, which has only examined erosion performance under fixed conditions. It innovatively integrates varying slurry concentrations and impingement angles using Taguchi and Response Surface Methodology (RSM) to optimize minimum erosion conditions. Furthermore, it adopts a practical approach by incorporating environmental simulation contexts and linking surface characterization to statistical modeling. This comprehensive method provides an enhanced understanding of erosion mechanisms and offers predictive tools for turbine maintenance planning in real-world situations. By linking ideas between various disciplines, the study promotes cross-disciplinary cooperation, innovation, and practical applications, eventually leading to enhanced performance, safety, and sustainability in biomedical and engineering settings affected by slurry erosion concerns.

Materials and methods

The methodology adopted for the proposed work is illustrated in Fig. 1.

Selection of substrate material

Table 1 shows the chemical composition of a material selected for this research work. CF8M samples of dimensions 16 mm × 16 mm × 6 mm were produced from steel flat. Before applying the coating, already samples were polished and cleaned with emery paper down to 800 grains to get the best adhesion possible between the coating and the substrate. After that, the necessary number of samples were coated with thick layers of Cr_3C_2-NiCr and WC-Co coatings using the Detonation Gun (D-gun) thermal spray procedure (Table 1). Chemical composition (wt.%) of CF8M (ASTM A743).

Coating powders

After a thorough literature survey, two different coatings were selected: WC + 12Co and Cr3C2 + 25NiCr, using a process of D-gun spray. Studies show that the chosen coatings have outstanding wear resistance and bond strength. The following qualities are included in the coating powder used, as shown in Table 2.

Deposition of coating by detonation spray process

Initially, the faces of the 16 mm by 16 mm CF8M samples were cleaned and polished using emery paper sanded down to 800 grains. To make the surface rougher and facilitate easier coating adhesion to the substrate, they were cleaned using an ultrasonic acetone cleaner. The chosen coating powders were then taken and applied to the steel samples using the D-gun spray method offered by SVX Surface-Engineering Pvt. Ltd in Greater Noida, India, by grasping the samples in an appropriate holder. The

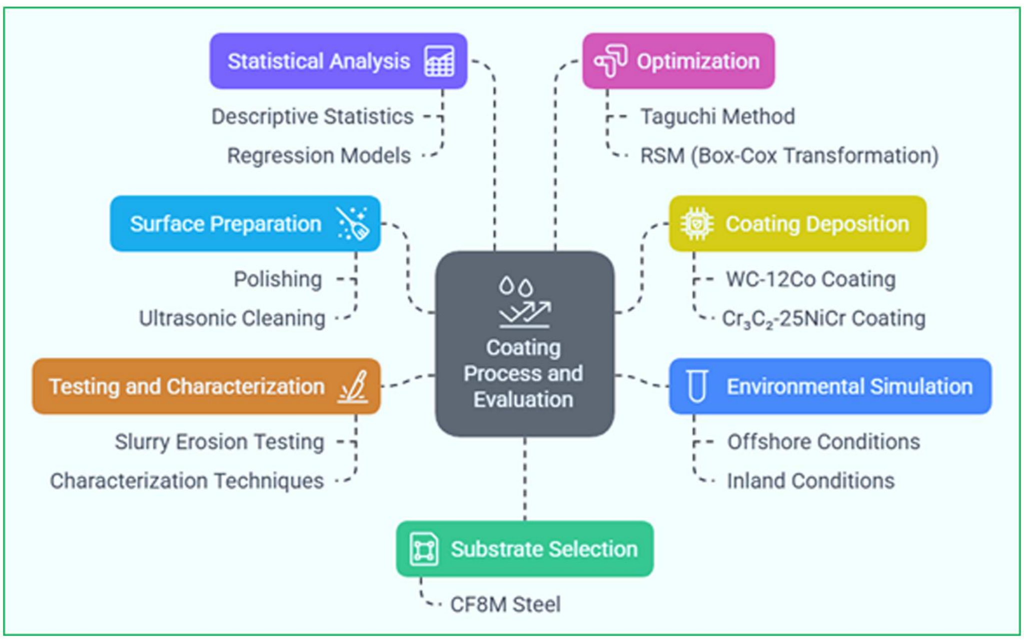

Figure 1. Experimental methodology for slurry erosion testing and optimization.

Table 1. Chemical composition (wt.%) of CF8M (ASTM A743).

Elements	C max	Si max	Mn max	S max	P max	Cr	Ni	Mo	Fe
Percentage (%)	0.08	1.5	1.5	0.04	0.04	17.0–210	9.0–130	2.0–30	Balance

Table 2. Coating powders details.

Powder	Percentage	Make and commercial code	Morphology	Grain size
WC-Co	WC-Co (88 : 12)	H C Starck; Amperit 518	Agglomerated, Sintered	15–45
Cr_3C_2-NiCr	Cr_3C_2-NiCr (75 : 25)	H C Starck; Amperit 584	Agglomerated, Sintered	10–45

Table 3. Detonation spray process parameters.

Fuel gas	Oxygen and acetylene
Carrier gas	Nitrogen
Oxygen flow rate (O_2)	2960 (WC); 2720 (Cr3C2NiCr)
Pressure	0.2 MPa
Acetylene flow rate (C_2H_2)	2400 (WC); 2320 (Cr3C2NiCr)
Pressure	0.14 MPa
Nitrogen flow rate (N_2)	720 (WC and Cr3C2NiCr)
Pressure	0.4 Mpa
Spray angle	90 degrees
Spray distance	165 mm
Max. substrate temperature	110 deg. C
No. of shots per second	3
Coating thickness per shot	5–25

following are the process parameters that the industry uses to deposit coatings, as shown in Table 3.

Design details of tester

The tester was constructed in the college workshop. A schematic of the slurry erosion tester is illustrated in Fig. 2. It depicts the experimental layout and component arrangement for better understanding of the flow dynamics, alignment, and positioning used during testing. It is made up of a sizable convergent-divergent slurry tank that is used to hold and move water. Steel 403 grade was used to make this. This cross-section's primary benefit is preventing particles from building up at the bottom of the tank, enabling slurry to circulate naturally due to gravity. It also includes a flat, mild steel bed with an appropriate holding arrangement. The middle groove of the bed allows the user to adjust the stand-off distance. A 90˚ bent MS flat serves as the workpiece holding fixture. There is a groove on the fixture face that faces the nozzle where a screw can be used to hold and modify the workpiece that follows the nozzle. The flatbed is bolted to the bottom face. Since the fixture lacks a mechanism for adjusting angles, it was altered for experimentation. Thus, certain adjustments were made to the fixture. The centrifugal pump inside the tester was driven by a 3 HP, 2800 rpm electric motor to circulate the slurry. A flow control valve regulated and controlled the pressure and flow in the slurry circulating pipes. A 3 mm diameter nozzle made of tungsten carbide was used to reduce its wear.

Variations in stand-off distance, flow pressure, velocity, incidence angle, and slurry concentration can be made with this tester. The hydro turbine and its parts accumulated silt and other particles from the Nathpa Jakhri Power Plant in Himachal Pradesh. After the silt was dried, the particle size was separated using sieve analysis. In addition, a specific amount of water was combined with silt with an average particle size of 300 μm to create three slurries. The slurries have a concentration of roughly 10 000, 15 000, and 20 000 ppm. Table 4 lists the test parameters employed, and Table 5 lists the different parameter sets applied to the uncoated, WC-Co, and Cr_3C_2-NiCr coated samples.

The selection of slurry concentration and impingement angle was made based on a combination of literature review, practical relevance to hydro-turbine operational conditions, and the need to explore the full spectrum of erosive behavior in coated and uncoated steel substrates.

- *Slurry Concentration (10 000 ppm, 15 000 ppm, 20 000 ppm):* These concentration levels were chosen to represent real-world operating environments encountered in hydroelectric power plants, particularly those located in sediment-rich regions such as the Himalayan belt. The silt-laden water in these areas often exhibits particle loadings in the range of 1%–2% by weight, which corresponds approximately to 10 000–20 000 ppm. This range enables us to assess the performance of protective coatings under varying erosive particle conditions, including low, moderate, and high levels.
- *Impingement Angles (30° and 90°):* The angles were selected to reflect the most critical scenarios of erosion in hydro-turbine components. 30° represents low-angle impacts, which are typically associated with sliding or cutting mechanisms and are most relevant for the erosion of ductile materials. 90° represents normal impact, corresponding to ploughing or fatigue mechanisms, and is more representative of brittle material erosion. These two angles also provide contrasting erosion modes, enabling a comprehensive evaluation of coating behavior under various impact dynamics.

Together, these parameters were selected to systematically investigate the combined influence of impact mechanics and abrasive particle loading, thereby simulating a wide range of realistic service conditions in slurry-exposed environments.

The choice of a 20 000 ppm slurry concentration and a 30° impingement angle was carefully guided by field observations from active hydroelectric power plants, as well as recognized trends in erosion studies from existing literature.

Results and discussion

The Scanning Electron Microscopy (SEM) and Energy Dispersive X-ray Analysis (EDAX) study of WC-Co and Cr_3C_2-NiCr coatings deposited via detonation gun spraying on CF8M stainless steel has been detailed, covering both eroded and non-eroded regions. Additionally, slurry erosion behavior and X-ray Diffraction (XRD)

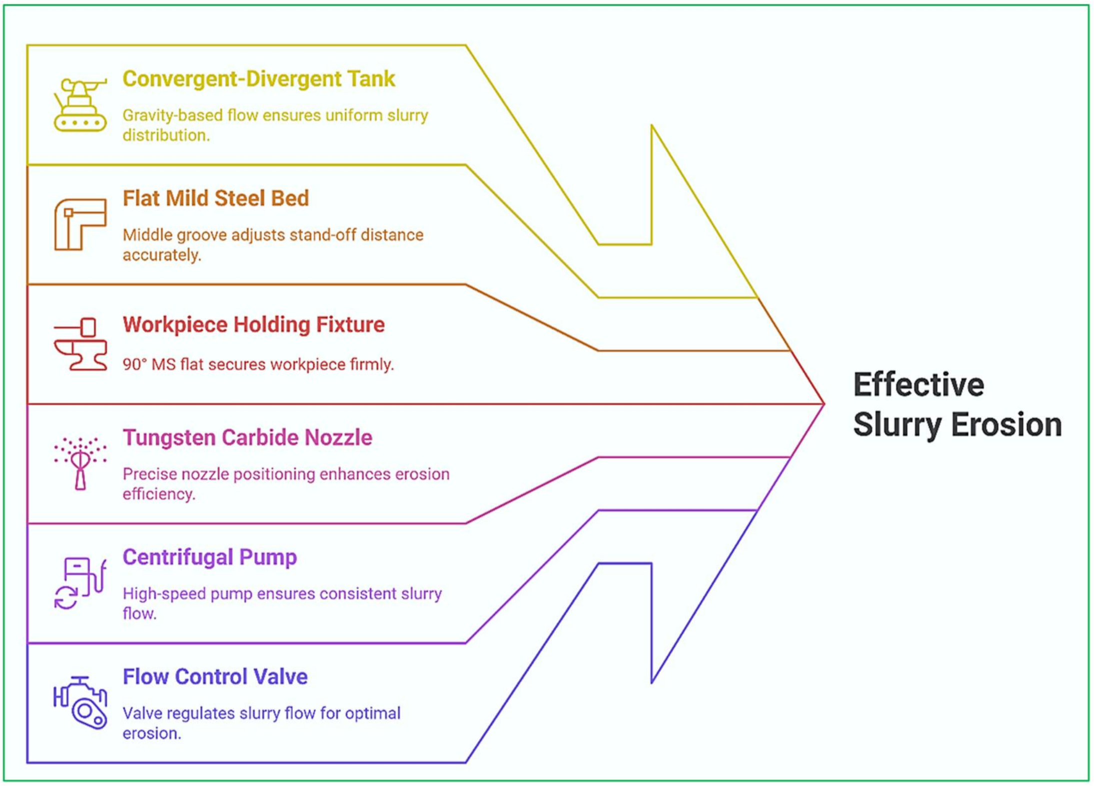

Figure 2. Schematic of the slurry erosion test setup.

Table 4. Parameters for slurry erosion testing.

Slurry conc. (ppm)	10 000	15 000	20 000
Impingement angle (degree)	30		90
Stand-off distance	15		
Pressure (psi)	25		
Time (h)	2		

Table 5. Set of parameters used during testing.

S. No./parameters	Slurry concentration (ppm)	Impingement (degree)
Set A	10 000	30
Set B	10 000	90
Set C	15 000	30
Set D	15 000	90
Set E	20 000	30
Set F	20 000	90

analysis of the coated surfaces are presented to further elucidate the coating performance and degradation mechanisms.

Coating characterization through visual examination

WC-Co-coated specimens look greyish upon visual inspection of D-gun coated specimens, while Cr_3C_2-NiCr samples seem silver greyish. Coating surfaces appear rough; no cracks were observed during visual examination.

The XRD pattern in Fig. 3a and b reveal the presence of WC, Co, and Cr3C2, NiCr. The patterns demonstrate the effective deposition of the planned coating materials, corresponding with predictions based on the selected materials. The distinct peaks corresponding to the crystalline structure of these components suggest a well-formed covering with a stable and defined structure. This structural integrity is crucial to the coatings' mechanical strength, wear resistance, and overall performance in severe conditions, making them ideal for applications that require robust surface protection.

Figure 3c and d depict the SEM/EDAX micrographs with elemental composition for the WC-Co and Cr_3C_2-NiCr detonation gun-coated specimens. The SEM/EDAX micrographs show a precise visual depiction of the coating morphology and elemental composition. The micrographs display homogeneity and uniformity, indicating an even distribution of the coating material with no apparent faults or abnormalities. This uniformity is crucial for ensuring consistent properties across the coated surface and the coatings' reliable performance and lifespan in practical applications. The lack of fractures or discontinuities confirms the integrity of the coatings, implying that they can withstand mechanical pressures and environmental variables without compromising their protective properties. The micrographs demonstrate the homogeneity, uniformity, and absence of cracks in the coatings. Oxygen (O) is present, indicating that the oxide formed during the detonation spraying process. Oxygen indicates that oxide compounds are forming during the detonation spraying process. By strengthening the coatings' resistance to oxidation and corrosion, these oxides can prolong their service life and preserve their protective qualities in harsh environments. Furthermore, developing oxide layers may enhance adhesion between the substrate and coating, thereby improving the overall stability and longevity of the coated components.

Ultimately, the quality, content, and structural integrity of the Cr_3C_2-NiCr and WC-Co coatings are fully validated by the findings of the SEM/EDAX micrographs and XRD patterns. These coatings possess the qualities necessary for high-performance surface protection in various industrial, automotive, and

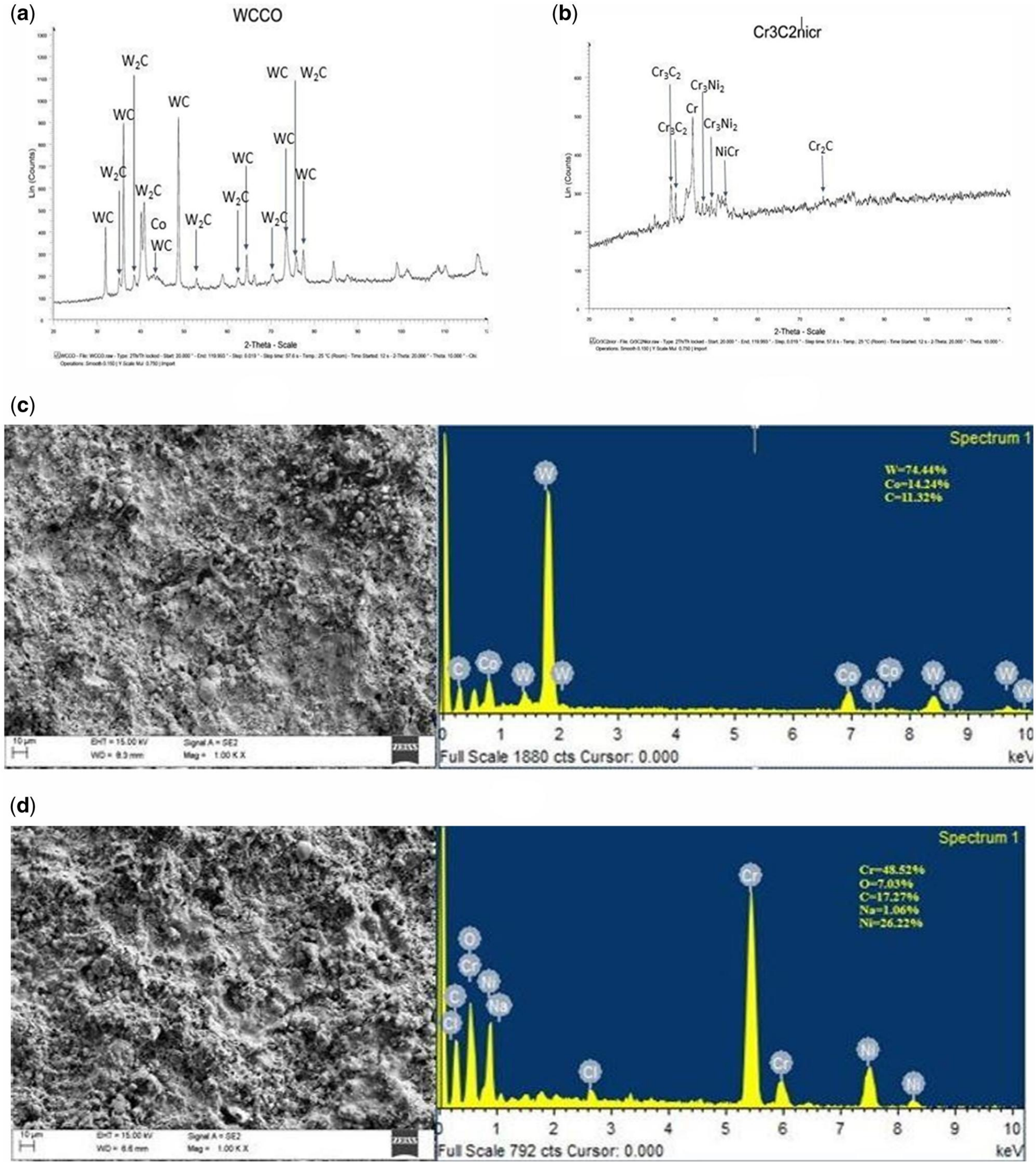

Figure 3. XRD pattern of (a) coated WC-Co (b) Cr_3C_2-NiCr on CF8M substrate; SEM/EDAX of (c)WC-CO (d) Cr_3C_2-NiCr as coated samples.

aerospace applications, among others. The comprehensive investigation and characterization of these coatings support their suitability for the intended uses, underscoring the importance of sophisticated materials characterization techniques in assessing coating performance and ensuring product reliability.

The XRD patterns (Fig. 4a and b) reveal distinct peaks that are consistent with the expected crystalline phases of the coating materials. For WC-Co, prominent peaks corresponding to hexagonal tungsten carbide and metallic cobalt confirm the presence of the primary coating constituents. The sharp and well-defined peaks suggest a high degree of crystallinity and phase stability retained during the detonation spray process. Similarly, the Cr_3C_2-NiCr-coated samples exhibit peaks corresponding to chromium carbide and a face-centered cubic (FCC) Ni-Cr matrix, indicating successful phase retention and proper alloying during deposition. The lack of amorphous humps or secondary unwanted phases suggests minimal decomposition or oxidation during spraying, which is critical for maintaining erosion resistance and coating durability.

Following testing, the specimens exposed to slurry erosion were weighed. The erosion or weight loss quantity equals the difference between the starting and final weight values. Table 6 shows all

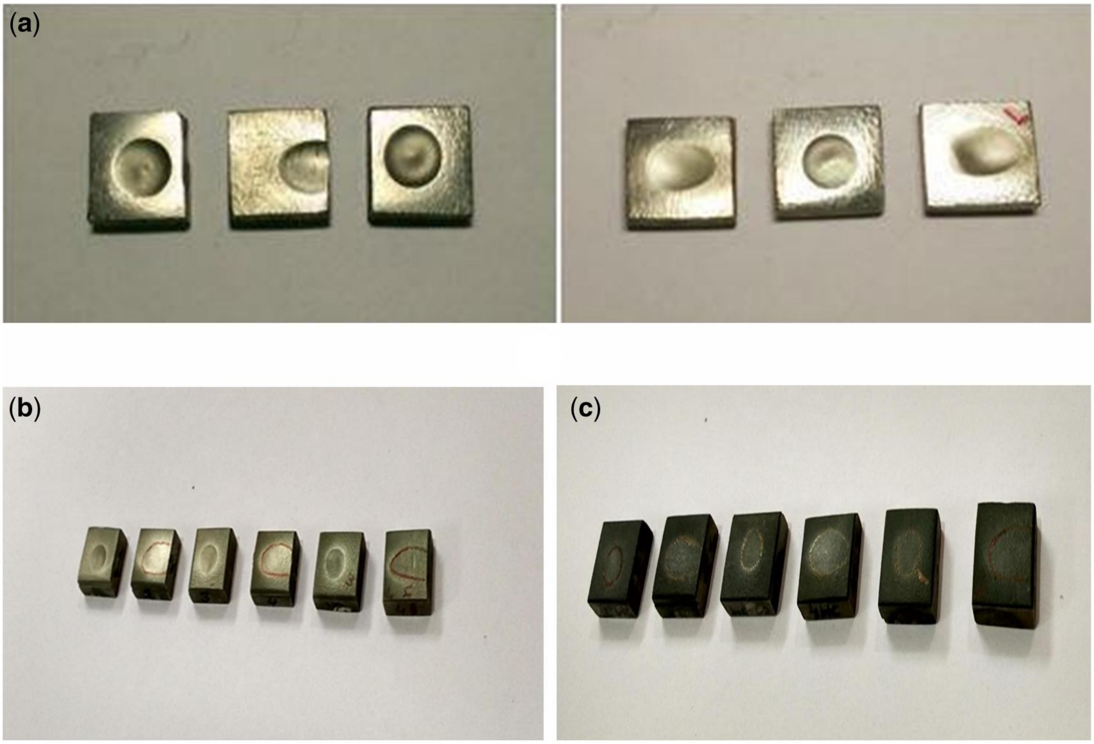

Figure 4. (a) Bare samples after the examination (b) Cr_3C_2-NiCr eroded samples (c) WC-Co eroded samples.

Table 6. Test results for slurry erosion.

Sample no.	Specimens	Slurry conc. (ppm)	Impingement angle (deg)	Initial weight (g)	Final weight (g)	Erosion/weight loss (g)
1	CF8M	10	90	12.221	12.132	0.089
2	Cr_3C_2-NiCr coated	10	90	12.267	12.227	0.04
3	WC-Co coated	10	90	12.569	12.554	0.015
4	CF8M	10	30	12.304	12.163	0.141
5	Cr_3C_2-NiCr coated	10	30	12.734	12.725	0.009
6	WC-Co coated	10	30	12.835	12.828	0.007
7	CF8M	15	90	12.51	12.37	0.14
8	Cr_3C_2-NiCr coated	15	90	12.604	12.574	0.03
9	WC-Co coated	15	90	12.618	12.598	0.02
10	CF8M	15	30	12.128	11.992	0.136
11	Cr_3C_2-NiCr coated	15	30	12.426	12.409	0.017
12	WC-Co coated	15	30	13.081	13.072	0.009
13	CF8M	20	90	11.376	11.231	0.145
14	Cr_3C_2-NiCr coated	20	90	12.192	12.13	0.062
15	WC-Co coated	20	90	12.79	12.74	0.05
16	CF8M	20	30	12.506	12.348	0.158
17	Cr_3C_2-NiCr coated	20	30	12.613	12.588	0.025
18	WC-Co coated	20	30	12.747	12.731	0.016

coated and uncoated specimens that experienced slurry erosion at different settings. There are circular impressions on the material surface due to the material being eroded from the center outward by a high-speed impingement jet. Only samples degraded at a 90° impingement angle exhibit visible circular impressions. When the impingement angle U is 30˚, the surface forms elliptical or U-shaped impressions. The slurry jet's passage in a specific direction could cause the elliptical marks. Weight loss due to slurry erosion trials is shown in Table 6. Compared to coated specimens, all CF8M specimens show a higher weight reduction. The table shows that for the CF8M specimen, the highest erosion occurs at a 30° impinged angle. The most outstanding erosion rates for ductile material were approximately 30˚ impingement angle, which explains this occurrence [40].

Table 6 demonstrates that the erosion rate increases for all specimens at an impact angle of 90° and with increasing slurry concentration. The highest degree of erosion happens on bare specimens, whereas the least amount occurs on WC-Co specimens. This difference in hardness between WC-Co and uncoated specimens can be explained. The following observations and trends were noted.

- ***Effect of Specimen Type***:
  The observed tendency for CF8M specimens to continually exhibit greater erosion rates than CR_3C_2-NiCr and WC-Co coated specimens emphasizes the protective effects of coatings in preventing erosion. CF8M, as an uncoated material, lacks the extra layers of protection that coatings offer. As a result, it is more vulnerable to the erosive pressures seen in

slurry settings, particularly at greater concentrations and impingement angles. In contrast, CR_3C_2-NiCr and WC-Co coatings are designed to endure erosive conditions. These coatings operate as barriers, absorbing and diffusing the energy of impacting particles in the slurry, thereby reducing the impact force on the substrate below. This protective mechanism significantly reduces erosion rates, as indicated by decreased weight loss in CR_3C_2-NiCr and WC-Co coated specimens under different test circumstances [41]. The erosion rates between CF8M and covered specimens demonstrate the need to apply protective coatings in erosive conditions. Coatings enhance the material's resistance to erosion, extending its useful life by reducing wear and deterioration. This protective function is crucial in the aerospace, automotive, and industrial industries, where components are subjected to rigorous working conditions [42].

- ***Impact of Slurry Concentration and Impingement Angle***:
  The effect of slurry concentration and impingement angle on erosion rates is crucial for understanding material behavior in erosive settings. Higher slurry concentrations result in a greater number of abrasive particles per unit volume, which increases the likelihood of material removal. Similarly, larger impingement angles provide more direct and violent contact between the slurry particles and the material surface, resulting in greater erosion effects [43]. The fact that CF8M specimens at 20 ppm and 30° impingement angle have greater erosion rates than the same material at lower concentrations or angles is consistent with these concepts. At 20 ppm, the slurry has a larger concentration of abrasive particles, accelerating the erosion process. The 30° impingement angle causes the slurry to flow more directly onto the material surface, increasing impact force and erosion rates. This phenomenon is critical in engineering applications that subject materials to abrasive media, such as hydraulic systems, pumps, and industrial gear. Understanding how slurry concentration and impingement angle affect erosion aids in creating better erosion-resistant materials and preventative measures [44].
  Slurry concentration directly affects the number of abrasive particles per unit volume of water. A higher concentration implies a denser population of solid particles, leading to more frequent collisions with the material surface during testing. This increased frequency of impact boosts the cumulative kinetic energy transfer to the coating. It accelerates material removal through mechanisms such as cutting, plowing, and fatigue-induced micro-fractures. Furthermore, at high concentrations, interactions between particles can enhance turbulence and intensify erosion effects. Therefore, the rise in erosion rate with slurry concentration reflects both the mechanical and dynamic nature of particle-surface and particle-particle interactions.
  The impingement angle plays a critical role in determining the erosion behavior of materials. At lower angles such as 30°, the abrasive particles tend to slide or glide along the surface, causing cutting, shearing, and plowing mechanisms typically associated with ductile material erosion. This results in higher erosion rates due to continuous surface deformation and removal of material layers. At 90°, the impact is more normal, resulting in plastic deformation, crater formation, and, in some cases, brittle fracture. In our study, the maximum erosion was observed at 30°, which is consistent with the ductile response of CF8M steel and the composite behavior of the sprayed coatings.
- ***Comparative Erosion Rates:***
  WC-Co coated specimens consistently show less erosion than CR_3C_2-NiCr coated specimens when comparing erosion rates between coated specimens. This demonstrates the better erosion resistance of WC-Co coatings under the test circumstances. The results reveal similar erosion patterns for each specimen type across all testing conditions [45]. This uniformity shows that the slurry erosion testing approach is reliable and repeatable. These findings are supported by the materials' known qualities and the protective mechanisms provided by coatings. CF8M is prone to erosion, particularly under high-velocity impacts like those used in slurry erosion experiments. In contrast, CR_3C_2-NiCr and WC-Co coatings are designed to enhance erosion, corrosion, and wear resistance, as evidenced by decreased erosion rates compared to CF8M [46].

The erosion rate significantly increased as the slurry concentration rose from 10,000 ppm to 20,000 ppm. This pattern is attributed to a higher density of abrasive particles in the slurry, resulting in more frequent impact events on the coated surface. At these elevated concentrations, the cumulative effect of particle collisions, along with increased kinetic energy transfer, intensifies cutting, micro-chipping, and surface fatigue mechanisms. While the coatings showed better resistance than the uncoated samples, the varying erosion levels across concentrations highlight the need to consider particle load in actual turbine conditions.

Descriptive statistics: erosion of specimens

Figure 5a provides statistical measures for erosion by WC-Co-coated specimens. The mean erosion value is calculated to be 0.01950, indicating the average amount of material lost due to erosion for WC-Co-coated specimens. The standard error of the mean is 0.00640, representing the variability of the sample mean from the population mean. The standard deviation of 0.01568 shows the spread or dispersion of erosion values around the mean. The variance, calculated as the square of the standard deviation, is 0.00025. These values suggest that the erosion data for WC-Co coated specimens are relatively consistent, with limited variability among the measurements. The minimum erosion value observed is 0.00700, indicating the smallest amount of material lost during erosion. The relatively low standard deviation and variance suggest that the erosion data is clustered around the mean with minimal dispersion.

Figure 5b provides CF8M specimens; the mean erosion value is calculated to be 0.13483, the standard error of the mean is 0.00967, and the standard deviation is 0.02369, showing the spread or dispersion of erosion values around the mean. The variance, calculated as the square of the standard deviation, is 0.00056. These values suggest that the erosion data for CF8M specimens have some variability around the mean but are relatively consistent overall. The minimum erosion value observed is 0.08900, with a first quartile of 0.12425, meaning that 25% of the erosion values fall below this threshold. The median erosion value (0.14050) is the data set's middle point, separating the erosion values' lower and upper halves. The maximum erosion value observed is 0.15800, representing the largest amount of material lost due to erosion.

Figure 5c depicts results for Cr_3C_2-NiCr coated specimens. The mean erosion value is calculated to be 0.03050, the standard error of the mean is 0.00765, and the standard deviation is 0.01875. The variance, calculated as the square of the standard deviation, is 0.00035. The minimum erosion value observed is 0.00900, and the median erosion value (0.02750) is the middle point of the data set, separating the lower and upper halves of erosion values. The

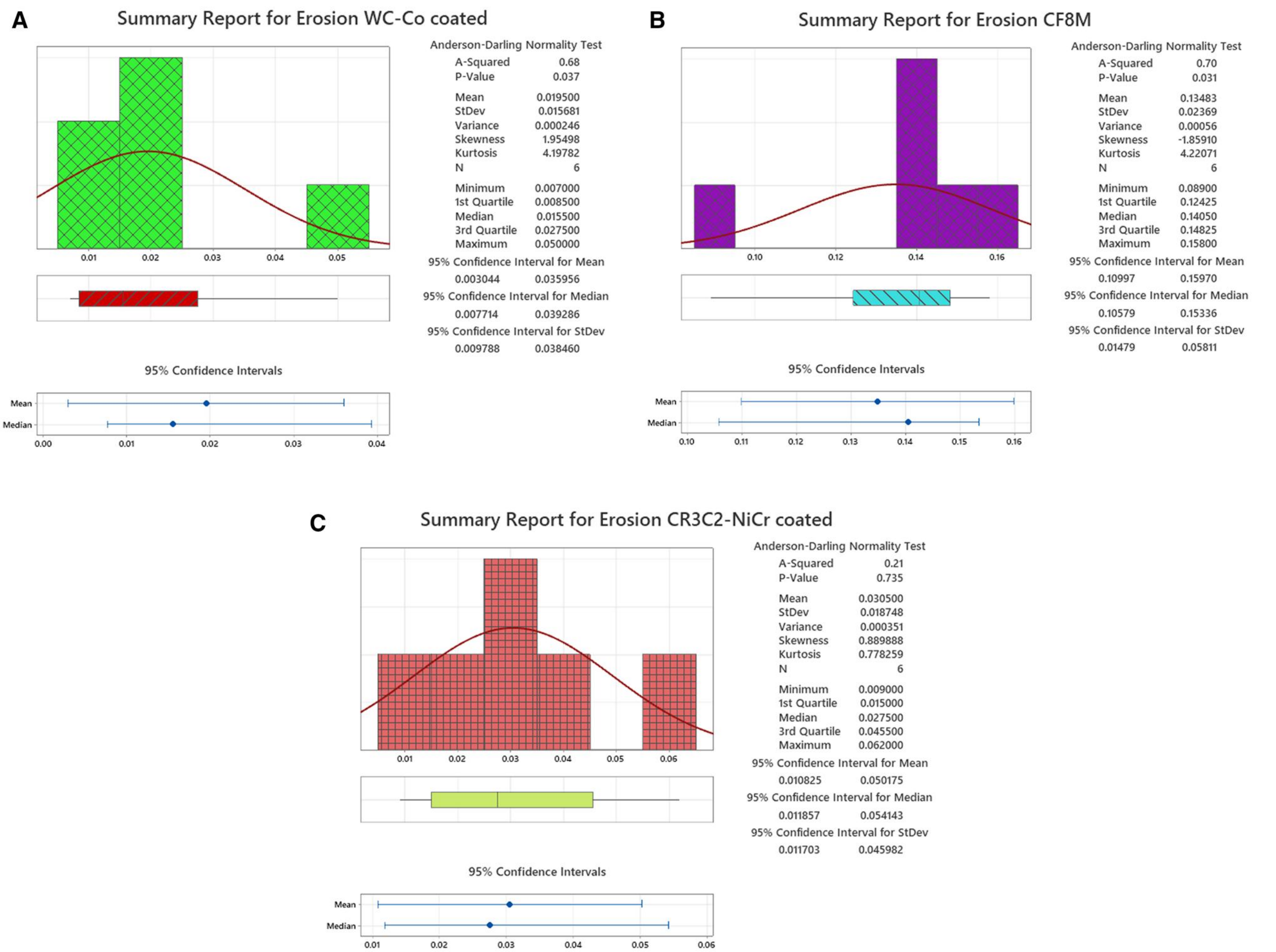

Figure 5. Descriptive statistics of erosion (a) Erosion WC-Co coated, (b) Erosion CF8M, (c) Erosion Cr_3C_2-NiCr coated.

third quartile is 0.04550, indicating that 75% of the erosion values are below this threshold. The maximum erosion value observed is 0.06200, representing the most significant amount of material lost due to erosion in the data set.

Comparing the results from the erosion data of WC-Co coated, CF8M, and Cr_3C_2-NiCr coated specimens reveals exciting insights into their erosion behavior. WC-Co-coated specimens exhibit relatively low and consistent erosion rates compared to CF8M and Cr_3C_2-NiCr coated specimens. CF8M specimens show the highest mean erosion rate and the widest spread of erosion values, indicating potentially higher erosion susceptibility. Cr_3C_2-NiCr coated specimens demonstrate moderate erosion rates with moderate variability around the mean. The choice of coating material significantly influences erosion behavior, with WC-Co coated specimens showing the most stable erosion performance among the three materials analyzed.

The median erosion value for the Cr_3C_2-NiCr-coated specimens was slightly lower than the mean, indicating a mild right skew in the erosion data. This suggests that while most samples exhibited moderate and consistent erosion, some extreme conditions, such as high slurry concentration combined with oblique impacts, resulted in a slightly more significant material loss. Nonetheless, the similarity between the mean and median indicates that the Cr_3C_2-NiCr coating exhibits stable and predictable performance, confirming its effectiveness for applications requiring operational consistency.

Regression analysis

The regression Equation (1) to Equation (3) shows the link between erosion rates and the independent variables of slurry concentration and impingement angle for WC-Co coated, CF8M, and Cr_3C_2-NiCr coated specimens, respectively. The coefficients (0.002200, 0.00365, and 0.00190) show the change in erosion rate per unit change in slurry concentration. The coefficients (0.000294, −0.000339, and 0.000450) indicate the change in erosion rate per unit change in impingement angle. These regression equations can be used to estimate erosion rates for each type of covered specimen based on specific slurry concentrations and impingement angles. They shed light on how these variables impact erosion behavior and may be utilized for predictive modeling and optimization in erosion resistance investigations.

$$\text{Erosion WC–Co coated} = -0.0312 + 0.002200\ \text{Slurry Concentration} + 0.000294\ \text{Impingement Angle} \tag{1}$$

$$\text{Erosion CF8M} = 0.1004 + 0.00365\ \text{Slurry Concentration} - 0.000339\ \text{Impingement Angle} \tag{2}$$

$$\text{Erosion } Cr_3C_2\text{–NiCr coated} = -0.0250 + 0.00190\ \text{Slurry Concentration} + 0.000450\ \text{Impingement Angle} \tag{3}$$

The regression analysis results from Table 7 reveal essential information about the parameters impacting erosion rates for

Table 7. Regression analysis results for erosion rates of specimens.

Term	Coef	SE coef	T-value	P-value	VIF
Erosion WC-Co coated					
Constant	−0.0312	0.0169	−1.85	.162	
Slurry concentration	0.002200	0.000961	2.29	.106	1.00
Impingement angle	0.000294	0.000131	2.25	.110	1.00
Erosion CF8M					
Constant	0.1004	0.0296	3.39	.043	
Slurry concentration	0.00365	0.00169	2.16	.119	1.00
Impingement angle	−0.000339	0.000230	−1.48	.237	1.00
Erosion CR_3C_2-NiCr coated					
Constant	−0.0250	0.0176	−1.42	.252	
Slurry concentration	0.00190	0.00100	1.89	.155	1.00
Impingement angle	0.000450	0.000137	3.29	.046	1.00

WC-Co coated, CF8M, and Cr_3C_2-NiCr coated specimens. For WC-Co coated specimens, the constant term of −0.0312 represents the predicted erosion rate when both the slurry concentration and the impingement angle are zero. However, the coefficients for slurry concentration (0.002200) and impingement angle (0.000294) are not statistically significant at the 0.05 alpha level, implying that the link between these factors and erosion rate is unknown based on the available data. In the case of CF8M specimens, the constant term 0.1004 indicates the predicted erosion rate at zero slurry concentration and impingement angle. The coefficients for slurry concentration (0.00365) and impingement angle (−0.000339) are likewise not statistically significant, showing that the impact of these factors on the erosion rate for CF8M coatings is uncertain.

In contrast, for Cr_3C_2-NiCr coated specimens, the constant term of −0.0250 represents the baseline erosion rate without slurry concentration and impingement angle effects. The coefficient for slurry concentration (0.00190) is not statistically significant, while the coefficient for impingement angle (0.000450) is at the 0.05 alpha level, indicating that impingement angle has a noticeable effect on erosion rate for Cr_3C_2-NiCr coatings. While the regression equations predict erosion rates based on slurry concentration and impingement angle, the coefficients' significance levels vary across coating types, highlighting the complexity of erosion behavior and the need for additional research to elucidate these relationships more conclusively.

Table 8 illustrates the ANOVA results for erosion rates of WC-Co coated, CF8M, and Cr_3C_2-NiCr coated specimens as a function of slurry concentration and impingement angle. For WC-Co coated specimens, the regression model, which includes slurry concentration and impingement angle, has a non-significant F-value of 5.15 and a P-value of .107, suggesting that the entire model does not explain erosion rate variability. Individually, slurry concentration and impingement angle show non-significant F-values and p-values, indicating that these variables do not significantly contribute to the variability in erosion rates for WC-Co-coated specimens. For CF8M specimens, the regression model yields a non-significant F-value of 3.43 and a P-value of .168, suggesting that it does not explain erosion rate variability. Individual F-values and P-values for slurry concentration and impingement angle are likewise non-significant, indicating that they have no meaningful impact on erosion rates for CF8M specimens. For Cr_3C_2-NiCr coated specimens, the regression model has a significant F-value of 7.20 and a P-value of .072, showing that the model somewhat explains the variability in erosion rates, albeit the significance level is minor. When analyzed independently, the impingement angle shows a significant F-value of 10.83 and a P-value of .046, indicating that the impingement angle substantially influences erosion rates for Cr_3C_2-NiCr coated specimens. The ANOVA results show that the impingement angle is more critical in explaining erosion rate variability than slurry concentration for Cr_3C_2-NiCr coated specimens. In contrast, neither slurry concentration nor impingement angle significantly explains erosion rate variability for WC-Co coated and CF8M specimens.

Table 8. ANOVA results for erosion rates of specimens.

Source	DF	Adj SS	Adj MS	F-value	P-value
Erosion WC-Co coated					
Regression	2	0.000952	0.000476	5.15	.107
Slurry concentration	1	0.000484	0.000484	5.24	.106
Impingement angle	1	0.000468	0.000468	5.06	.110
Error	3	0.000277	0.000092		
Total	5	0.001230			
Erosion CF8M					
Regression	2	0.001952	0.000976	3.43	.168
Slurry concentration	1	0.001332	0.001332	4.68	.119
Impingement angle	1	0.000620	0.000620	2.18	.237
Error	3	0.000854	0.000285		
Total	5	0.002807			
Erosion CR_3C_2-NiCr coated					
Regression	2	0.001454	0.000727	7.20	.072
Slurry concentration	1	0.000361	0.000361	3.57	.155
Impingement angle	1	0.001093	0.001093	10.83	.046
Error	3	0.000303	0.000101		
Total	5	0.001757			

The regression equations produced in this study provide more than mere statistical insights; they serve as essential predictive tools for practical hydro-turbine applications. By analyzing erosion behavior in relation to slurry concentration and impingement angle, these models enable plant operators to anticipate erosion across various sediment loads and flow conditions. This capability enables proactive maintenance planning and enhanced optimization of operating schedules during periods of high silt. Additionally, understanding the varying responses of coatings, such as WC-Co and Cr_3C_2-NiCr, to these factors can guide more efficient material choices for components subjected to specific erosive environments. Incorporating these models into predictive maintenance frameworks or digital twin systems can enhance decision-making, minimize unexpected downtime, and prolong the lifespan of components, ultimately improving the economic and operational efficiency of hydroelectric facilities.

The regression models for WC-Co and Cr_3C_2-NiCr coatings yielded high F-values and low p-values ($P < .001$), indicating strong statistical significance. Their respective R^2 values exceeded 92%, demonstrating that the models can explain a large portion of the variability in erosion rate as a function of slurry concentration and impingement angle. The model for CF8M steel also demonstrated meaningful predictive power, albeit with slightly more significant variability due to the absence of protective coatings and a wider range of material responses. These results confirm that the regression models are robust and suitable for process optimization and predictive erosion analysis under varied operational conditions.

Optimization of erosion by the taguchi method and response surface modelling (RSM): customized design

The Taguchi technique [47, 48] and RSM [49, 50] are used to optimize erosion. Table 6 was used as a customized design inside

Table 9. ANOVA for SN ratios and means of erosion.

Source	DF	Seq SS	Adj SS	Adj MS	F	P
SN ratios						
Specimen	2	1130.6	1130.6	565.31	47.16	.000
Slurry concentration	2	109.9	109.9	54.96	4.58	.033
Impingement angle	1	111.2	111.2	111.21	9.28	.010
Residual error	12	143.8	143.8	11.99		
Total	17	1495.6				
S		**R-Sq**				**R-Sq(adj)**
3.4623		90.38%				86.37%
Means						
Specimen	2	0.048616	0.048616	0.024308	85.35	0.000
Slurry concentration	2	0.002080	0.002080	0.001040	3.65	0.058
Impingement angle	1	0.000296	0.000296	0.000296	1.04	0.328
Residual error	12	0.003418	0.003418	0.000285		
Total	17	0.054410				
S		**R-Sq**				**R-Sq(adj)**
0.0169		93.72%				91.10%

Minitab. This method combines the Taguchi method for robust parameter design with RSM to enhance erosion resistance. Minitab can be used to develop and evaluate customized designs, enabling quick parameter exploration and determining the optimal settings for minimizing erosion. This methodology combines the characteristics of experimental design techniques with statistical analysis to improve erosion performance in coated specimens.

Taguchi method analysis of erosion

Table 9 depicts results for ANOVA for means and Signal-to-Noise Ratio (SN ratios) of erosion. The data analysis includes investigating the correlations between SN ratios, erosion methods, and different affecting variables such as specimen type, slurry concentration, and impingement angle. Significant coefficients were identified when analyzing SN ratios. Specimen 1 had a significant negative influence on SN ratios, resulting in lower ratios than the baseline, but Specimen 2 had a favorable effect, increasing SN ratios. The slurry concentration of 10 ppm and an impingement angle of 30 degrees substantially affected SN ratios. The high coefficient of determination (R-squared) of 90.38% suggests that the model accounts for a significant percentage of the variability in SN ratios. The ANOVA findings emphasized the importance of these parameters. Both SN ratios and means of erosion were strongly impacted by specimen type, with slurry concentration having a considerable effect on SN ratios but only a marginally significant impact on means of erosion. The impingement angle was also important in SN ratios, and it tended to be substantial for erosion paths. The residual errors and total sums of squares represented unexplained variability in the data and overall variability, respectively. Significant coefficients were found again when the means of erosion were analyzed. Specimen 1 had a favorable influence on erosion rates, but Specimen 2 had a negative impact. Slurry concentration and impingement angle had little effect on erosion methods, exhibiting a lower influence compared to specimen types. The model summary displays a high R-squared value of 93.72%, indicating a strong relationship between the predictors and the mean erosion values. These analyses explain how specimen kinds, slurry concentration, and impingement angle affect SN ratios and erosion mechanisms. They highlight essential elements that influence erosion behavior and aid in understanding the dynamics of erosion resistance in the specimens under study.

The Taguchi method was chosen for its ability to assess multiple parameters efficiently with fewer experiments, utilizing an orthogonal array to create balanced comparisons across various levels [51, 52]. The "smaller-the-better" SN ratio was specifically selected to minimize variability in erosion rates and identify settings that consistently minimize wear under variable slurry conditions. In contrast to a full factorial design, the Taguchi approach is more feasible when experimental resources are restricted, yet it still provides statistically meaningful optimization insights. Its combination with RSM improves accuracy by capturing interaction effects and nonlinear behavior. Although initial normality tests indicated minor deviations, an ANOVA was conducted based on its known robustness to non-normal data [53, 54], and a Box-Cox transformation was applied to improve the distributional assumptions during RSM.

The ANOVA results for both SN ratios and erosion means (Table 9) indicate that specimen type has the most significant influence on erosion performance and variability, accounting for the most important percentage contribution to the total variance. This highlights the crucial role of material properties in determining erosion resistance. The impingement angle emerged as the second most influential factor, consistent with its effect on erosion mechanisms, precisely the distinction between cutting and impact. Slurry concentration, while still impactful, contributed less to the overall variability. The similarity in factor ranking between the SN and mean analyses suggests that optimizing material selection has the most substantial impact on both minimizing erosion and improving robustness across operational conditions.

The ANOVA results reveal material-specific variations in how operational factors affect erosion. For uncoated CF8M steel, slurry concentration was the primary factor influencing the erosion rate, which aligns with expectations given the material's direct exposure to abrasive particles. Conversely, Cr_3C_2-NiCr-coated specimens exhibited a statistically significant reaction to impingement angle ($P = .046$), highlighting their sensitivity to directional impacts due to the brittle nature of chromium carbide phases. Meanwhile, WC-Co coatings exhibited a more balanced response to both slurry concentration and impingement angle, reflecting the toughness and ductility of the cobalt matrix, alongside the hardness of the tungsten carbide particles. These results underscore that a coating's effectiveness stems not only from its erosion resistance but also from its adaptability to various operational conditions.

The main effects plot for erosion is shown in Fig. 6a for means and Fig. 6b for SN ratios, indicating that specimen 3, with a slurry concentration of 10 ppm and an impingement angle of 30°, yields an optimal erosion rate of 0.007 g. The investigation highlights the critical aspects of achieving the best erosion resistance, providing valuable insights for enhancing erosion performance in the analyzed specimens.

The main effects plot for SN ratios distinctly highlights the factor level combinations that enhance erosion resistance. The optimal SN ratio, signifying minimal erosion and maximum durability, was achieved using the WC-Co coating with a 10 000 ppm slurry concentration at a 90° impingement angle. This indicates that standard impact conditions, combined with a low abrasive load and a complex, ductile coating, yield the best performance. Uncoated steel, increased slurry concentrations, and angled impacts were associated with lower SN ratios, indicating poorer erosion and more significant variability in response. These findings strongly support the selection of specific operating and

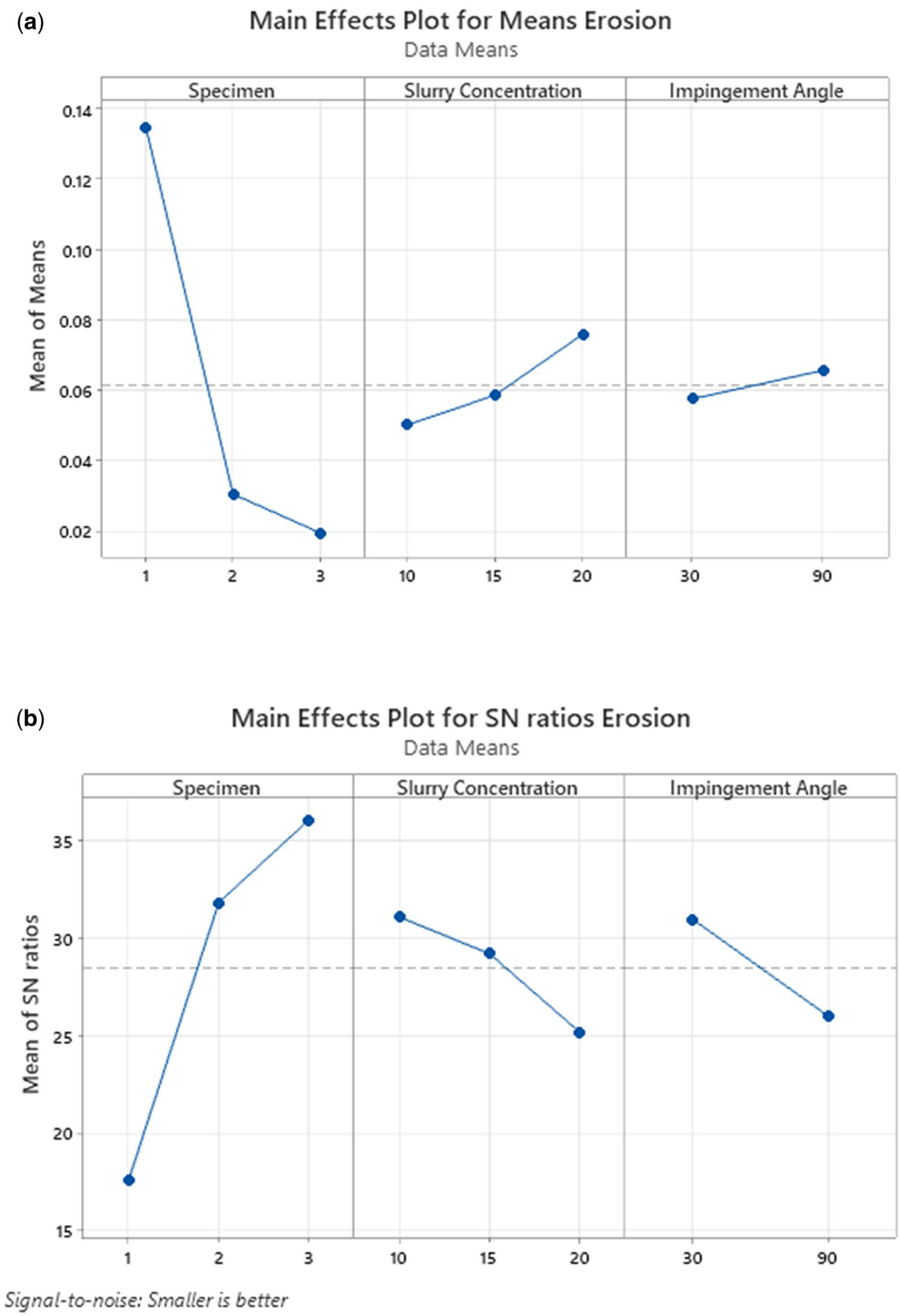

Figure 6. Main effects plots (a) means, (b) SN ratios.

material conditions to enhance durability in environments exposed to slurry.

The SN ratios, determined using the "smaller-the-better" approach, serve as a reliable indicator of process stability and resistance to erosion across various factor settings. By evaluating the average SN ratios for different levels of each influencing factor, such as specimen type, slurry concentration, and impingement angle, the Taguchi method reveals which parameters significantly impact the erosion results. A more significant delta (the difference between the maximum and minimum SN, refer to Fig. 6b) indicates a more substantial influence of a factor. In this research, specimen type showed the highest delta, suggesting that material properties are crucial for controlling erosion. While the impingement angle and slurry concentration also played a role, their impact was less significant. These results validate the relationship between erosion mechanisms and both material composition and impact conditions, underscoring the effectiveness of SN analysis in enhancing system performance.

The Taguchi analysis showed that specimen type greatly influenced both the average erosion rates and the SN ratios. Among the three materials tested, the WC-Co coated specimens had the lowest average erosion rates and the highest SN ratios, demonstrating not only excellent erosion resistance but also reliable performance across varying testing conditions. The Cr_3C_2-NiCr coatings provided better protection than uncoated steel but presented somewhat more variability, as evidenced by their lower SN ratios compared to WC-Co. The uncoated CF8M steel experienced the highest erosion and exhibited the least process robustness, underscoring the necessity for protective coatings in erosive environments. These findings highlight the importance of specimen type as a key factor in minimizing material loss and improving coating performance.

In contrast to the Taguchi method, which focuses on main effects through its orthogonal design, the RSM approach incorporates interaction and quadratic terms to provide a more comprehensive examination of parameter interdependencies and nonlinear effects.

Response surface modelling (RSM) of erosion

In the RSM analysis for erosion, the model was built using ‘Specimen’, ’Slurry Concentration,’ and ‘Impingement Angle’ variables using Minitab software and utilizing the customized design. However, the variable “Impingement Angle*Impingement Angle” was excluded from the analysis since it could not be approximated. In addition, the data underwent a Box-Cox transformation. The rounded lambda value, which reflects the transformation type, equals zero, indicating a logarithmic transformation. However, the projected lambda value (which optimizes the transformation for normalcy) is 0.138195. This minor divergence from the rounded lambda implies a subtler adjustment to reach the necessary normalcy. The 95% confidence interval for lambda was (-0.477305, 0.717695), showing the degree of ambiguity in the transformation’s exact nature. This interval implies that the transformation may need more than a simple logarithmic adjustment, with possible differences in the transformation strategy based on the data’s features. Overall, the Box-Cox transformation with an estimated lambda of 0.138195 falls within the confidence interval of (-0.477305, 0.717695), indicating the need for a transformation that moderately adjusts the data to improve normality while accounting for the uncertainty inherent in the transformation process.

Equation (4) depicts erosion in uncoded units and describes the logarithm of erosion as a function of Specimen, Slurry Concentration, Impingement Angle, and their interactions. Each coefficient in Equation (4) represents the impact of the corresponding variable on erosion rates after accounting for other factors. A higher Specimen value (a negative coefficient of −4.448) correlates with lower erosion rates. Slurry Concentration (with a coefficient of −0.157) and Impingement Angle (coefficient of −0.0097) also contribute to reducing erosion. Interaction terms, such as Specimen*Specimen and Specimen*Slurry Concentration, indicate combined effects that further influence erosion rates.

$$\begin{aligned}\ln(\text{Erosion (g)}) = 2.44 \\ &-4.448\ \text{Specimen} - 0.157\ \text{Slurry Concentration} \\ &-0.0097\ \text{Impingement Angle} + 0.577\ \text{Specimen} * \text{Specimen} \\ &+0.00495\ \text{Slurry Concentration} * \text{Slurry Concentration} \\ &+0.0357\ \text{Specimen} * \text{Slurry Concentration} \\ &+0.00894\ \text{Specimen} * \text{Impingement Angle} \\ &+0.000093\ \text{Slurry Concentration} * \text{Impingement Angle}\end{aligned} \tag{4}$$

ANOVA in Table 10 examines the effects of Specimen, Slurry Concentration, Impingement Angle, and their interactions on the transformed response variable erosion. The whole model has a remarkable degree of significance, with a high F-value of 27.22 and a matching *P*-value of .000, showing that the erosion model collectively explains a significant percentage of the variability shown in the transformed erosion response. ‘Specimen’, ‘Slurry Concentration’, and ‘Impingement Angle’s’ linear effects significantly contribute to erosion rates, as indicated by their low p-values (all less than 0.01) and considerable F-values ranging from 15.97 to 63.00. Among these parameters, the ‘Specimen’ has the most linear influence on erosion. Furthermore, the introduction of square and interaction variables in the model reveals new levels of complexity. The square term’s substantial *P*-value (.010) suggests a potential nonlinear link between some parameters and erosion, implying that their influence may not be linear.

The important interaction terms, such as Specimen*Specimen, Specimen*Impingement Angle, and 2-Way Interaction, demonstrate the combined influence of these parameters on erosion rates, emphasizing the need to consider their joint effects. The error component in the ANOVA table

Table 10. Analysis of variance for transformed response erosion.

Source	DF	Adj SS	Adj MS	F-value	P-value
Model	8	19.0370	2.3796	27.22	.000
Linear	3	16.5220	5.5073	63.00	.000
Specimen	1	13.6523	13.6523	156.18	.000
Slurry Concentration	1	1.3957	1.3957	15.97	.003
Impingement Angle	1	1.4740	1.4740	16.86	.003
Square	2	1.3950	0.6975	7.98	.010
Specimen*Specimen	1	1.3338	1.3338	15.26	.004
Slurry Concentration*Slurry Concentration	1	0.0612	0.0612	0.70	.424
2-Way Interaction	3	1.1200	0.3733	4.27	.039
Specimen*Slurry Concentration	1	0.2552	0.2552	2.92	.122
Specimen*Impingement Angle	1	0.8625	0.8625	9.87	.012
Slurry Concentration*Impingement Angle	1	0.0024	0.0024	0.03	.873
Error	9	0.7867	0.0874		
Total	17	19.8237			

Model summary for transformed response

	S	R-sq	R-sq(adj)	R-sq(pred)
	0.295654	96.03%	92.50%	84.29%

indicates the unexplained variation in erosion rates, which is minor compared to the total variability captured by the erosion model, as shown by the total sum of squares. This mismatch suggests that the model accurately accounts for a considerable percentage of the observed erosion variability.

To fulfill the requirements of normality and homoscedasticity in the RSM regression analysis, the erosion rate data underwent a Box-Cox transformation. This step was essential due to slight deviations from normality found in the residuals, as confirmed by the Anderson-Darling test. The Box-Cox method identified the optimal power transformation to stabilize variance and improve the linearity of the model fit. Consequently, the transformed model demonstrated greater accuracy, with residuals exhibiting a more uniform distribution, and ANOVA results indicating high significance ($P < .001$), thereby confirming the reliability of the predictive regression equation.

The summary statistics demonstrate the model's robustness, with a high coefficient of determination (R-squared) of 96.03%. The adjusted R-squared (92.50%) and anticipated R-squared (84.29%) results further demonstrate the erosion model's ability to explain and forecast erosion rates depending on specimen, slurry concentration, impingement angle, and their interactions. The findings highlight the profound interactions between these parameters and their significant contributions to the modified erosion response, providing valuable insights into understanding and improving erosion behavior in the examined specimens.

Among the analyzed regression coefficients, the impingement angle for the Cr_3C_2-NiCr coating (Table 8) was found to be statistically significant at the 0.05 alpha level ($P = .046$), highlighting its strong impact on the erosion rate. Although some individual coefficients had P-values exceeding 0.05, likely due to the limited degrees of freedom in the Taguchi-based design, the overall model in the RSM analysis (Table 10) demonstrated high robustness ($P < .001$), with R^2 values above 92%. This indicates that both slurry concentration and impingement angle, especially their interaction, are crucial in influencing the erosion response. Thus, even if not all variables achieve individual significance, the models remain helpful for prediction and optimization purposes.

The individual F-values in the ANOVA tables represent the relative influence of slurry concentration and impingement angle on erosion rate. A higher F-value indicates that a particular factor contributes more significantly to the variability in the response variable. The corresponding p-values assess whether these effects are statistically significant. For instance, in the Cr_3C_2-NiCr-coated samples (Table 8), the impingement angle had a P-value of .046, confirming its important role at the 0.05 level. Similarly, in the RSM analysis (Table 10), both factors, along with their interaction, were highly significant ($P < .001$), as supported by elevated F-values. These results confirm that slurry concentration and impingement angle are key parameters that significantly influence erosion performance, and must be carefully considered in coating design and system optimization.

The model's R-squared value of 90.38% based on SN ratios indicates that the experimental factors specimen type, slurry concentration, and impingement angle account for most of the variability in erosion behavior. This notable figure attests to the model's robust predictive ability and statistical precision. Additionally, it implies that the chosen parameters effectively correspond to the fundamental erosion mechanisms, allowing for confident optimization of performance and durability in real-world applications.

As the slurry concentration increased from 10 000 ppm to 20 000 ppm, the average erosion rate rose steadily across all samples due to the higher density of abrasive particles striking the surface. However, the impact on SN ratios varied by material. The WC-Co and Cr_3C_2-NiCr coatings showed relatively higher SN ratios, signifying stable erosion resistance even under challenging conditions. The CF8M steel experienced a significant drop in its SN ratio, indicating both increased material loss and performance inconsistency. This implies that while higher slurry concentrations exacerbate erosion, the response of a material, as reflected in its SN ratio, is heavily influenced by its coating integrity and resistance properties.

Figure 7a show a Pareto chart and residual plots for erosion analysis, as shown in Figure 7b. A Pareto chart displays the magnitude of various factors in descending order and shows the relative importance of different factors or variables influencing erosion rates. The bars in the chart are sorted from the most significant to the least important based on their impact on erosion. Residual plots are used to assess the goodness of fit of a regression model. The residual plots for erosion display how well the regression model fits the actual erosion data. Patterns in the residuals, random scattering around zero, indicate a good fit, while systematic patterns suggest issues like heteroscedasticity or nonlinearity in the model. A comprehensive view of the factors influencing erosion rates through the Pareto chart assesses the model's performance and potential areas for improvement through the residual plots.

The RSM analysis confirmed that the specimen type, slurry concentration, and impingement angle have a significant impact on erosion. It also identified the best conditions to achieve minimal material loss. These insights provide a quantitative foundation for selecting coating materials and optimizing operational parameters in hydro-turbine systems. This practical application allows engineers to mitigate erosion damage by optimizing flow conditions and focusing coating efforts on areas with the highest erosion risk.

Although individual P-values in the regression models exceeded 0.05 due to the limited sample size, the models were still used to explore trends and generate predictive insights. The consistency of these trends with RSM and Taguchi analyses supports the overall conclusions drawn.

RSM is essential for advancing erosion analysis beyond simple parameter evaluation. By integrating both main effects and interaction terms, RSM facilitates the creation of a predictive model that effectively captures the nonlinear dynamics of erosion rates influenced by different slurry concentrations and impingement angles. The regression equation obtained from RSM enables the prediction of erosion performance over a broad range of parameters, thereby eliminating the need for additional experiments. Additionally, the optimization findings offer practical insights for minimizing erosion. The model's statistical significance ($P < .001$) and a high R^2 value (>92%) further affirm its effectiveness for predictive analysis and strategic planning in real-world scenarios.

SEM/EDAX analysis of eroded specimens

The surface morphologies of all eroded, coated, and uncoated samples were examined. EDAX analyses carried out at slurry concentrations of 20 ppm and impingement angles of 90° and 30° are shown in Figs 8–10. The study's micrographs distinctly display the appearance of fractures, craters, and cracks on the specimens' surfaces. The coating material uprooting creates the craters. The micrographs indicate that the erodent's cutting or plowing action is primarily responsible for material removal at lower impact angles. On the other hand, micro-cutting, fatigue,

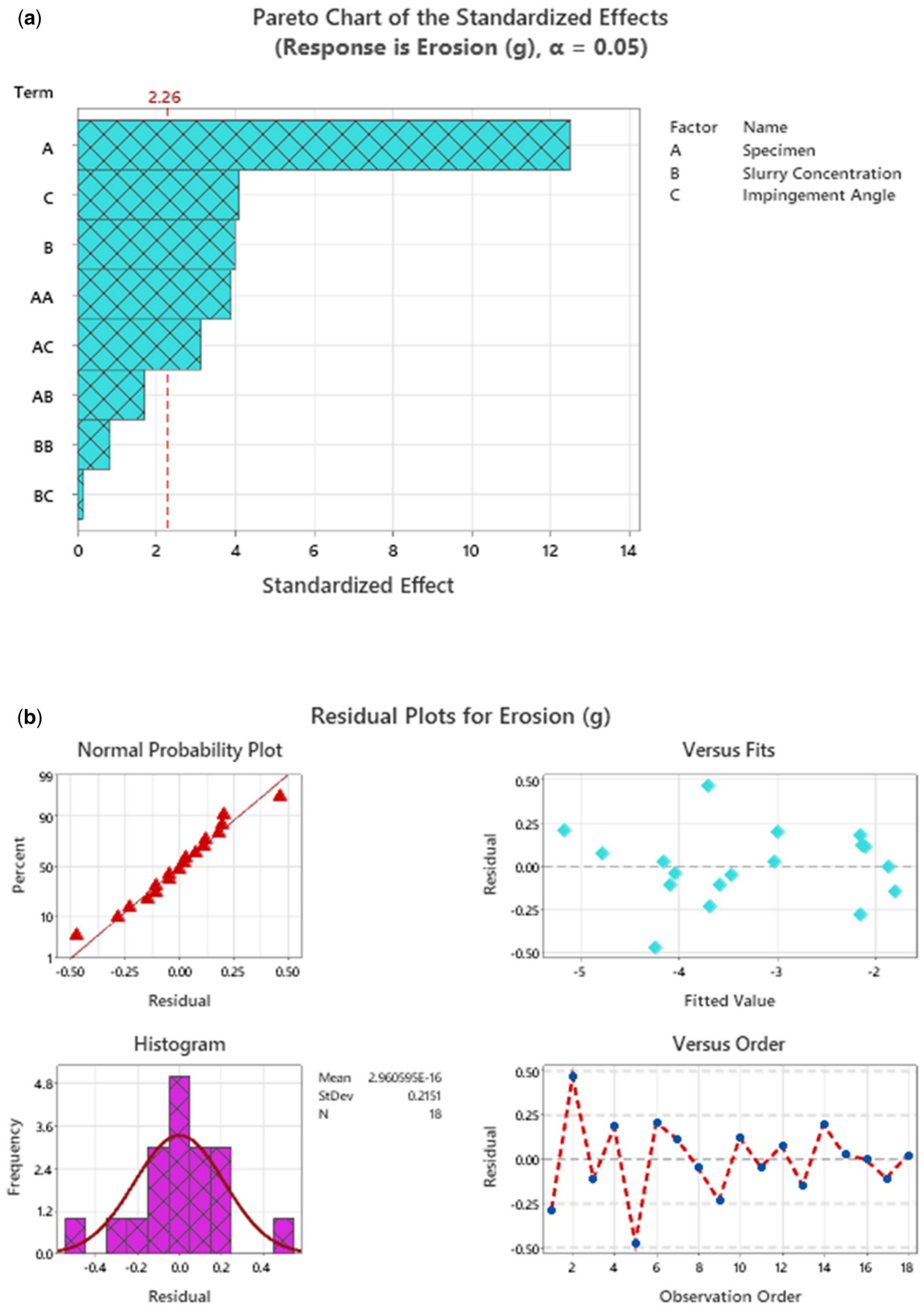

Figure 7. (a) Pareto chart, (b) residual plots for erosion.

and brittle cracking at normal impact angles could cause the material removal. Additionally, photos taken at higher magnification show that different metal oxides have formed on the surfaces of worn-out samples.

The EDAX spectra indicated that oxygen was present in both WC-Co and Cr_3C_2-NiCr coatings. This presence is likely a result of partial oxidation of molten or semi-molten particles during their trajectory through the high-temperature detonation flame. Even in controlled spraying conditions, brief contact with ambient oxygen can lead to the formation of surface oxides on the coating particles. This kind of oxidation is a typical characteristic of thermal spray processes, affecting properties such as porosity, adhesion, and hardness. Nevertheless, the observed oxygen levels were not significant and did not seem to affect the coating's erosion resistance or structural integrity.

Oxygen in coatings frequently contributes to the creation of thin oxide layers during thermal spraying. Specifically, oxides such as Cr_2O_3 found in Cr_3C_2-NiCr and Co-based oxides in WC-Co coatings act as passive protective barriers. These oxide layers minimize the diffusion of oxygen and corrosive elements into the coating matrix, thus improving oxidation and corrosion resistance. If their formation is controlled and uniform, these layers typically enhance the longevity of coated components used in harsh environments, like those encountered in hydro-turbines.

From experiments, it was revealed that altering the impingement angle and slurry concentration influences the erosion rate. It was revealed that when slurry concentration rises, so does the erosion rate. The Cr_3C_2-NiCr specimens with uncoated tungsten carbide and cobalt showed a material loss. This could be explained by the simultaneous brittle and ductile behavior of Cr_3C_2-NiCr [55].

In Fig. 8, the micrographs clearly show the imprint of fractures and the creation of craters on the specimen's surfaces. These markings imply that the erosive particles produced localized damage, with the uprooting of coated material resulting in craters. Lower impingement angles cause material removal due to the erodent's cutting or plowing motions, resulting in surface abrasion and material loss. Figure 9 shows a deeper look at the tiny features, exhibiting micro-cutting, fatigue, and brittle cracking processes contributing to material loss under typical impact angles. Various metal oxides on worn-out sample surfaces, seen at higher magnification, reflect chemical reactions or oxidation processes during erosion [56]. The experimental results support these observations, demonstrating that erosion rates rise with larger slurry concentrations.

Furthermore, the material loss for Cr_3C_2-NiCr is comparable to that of uncoated, tungsten carbide, and cobalt specimens, indicating its dual nature of showing both ductile and brittle behaviors concurrently. This behavior is critical for understanding how coatings and materials react to erosive environments, emphasizing the significance of material selection and design considerations in erosion-resistant applications [57]. Combining surface morphologies, EDAX analysis, and experimental data gives a thorough knowledge of erosion processes and material behavior under various erosive situations. These findings are useful in creating solutions to reduce erosion-related damage while improving the durability and performance of materials and components in erosive settings [58].

Implications of the study

The implications of this study extend to several critical areas in biomedical and engineering fields, with profound impacts on materials science, energy sustainability, and the performance of medical devices.

- *Materials Science Advancements:* This work sheds light on advanced materials engineering by examining the slurry erosion performance of WC + Co and CR3C2 + NiCr coatings on hydroturbine steel. Understanding how these coatings behave in erosive environments enhances our understanding of coating materials and informs the development of innovative, erosion-resistant materials. This has far-reaching consequences for various sectors, including aerospace, automotive, and marine engineering, where erosion-resistant materials are critical for component durability and performance.
- *Energy Sector Optimization:* In the context of hydropower generation, where slurry erosion causes considerable problems to turbine components, the study's findings directly impact improving energy output and lowering maintenance costs. Coatings with excellent erosion resistance can extend the life of turbine components, reduce downtime for maintenance and repairs, and contribute to more efficient and sustainable energy generation. This has far-reaching consequences for power system dependability and the economic feasibility of renewable energy sources.
- *Biomedical Device Durability:* The study's focus on biomedical applications has consequences for the longevity and performance of medical devices and implants. Understanding how coatings tolerate slurry erosion can help to create implant materials that are more durable in severe physiological settings. This is especially important for orthopedic implants, cardiovascular devices, and prostheses since long-term durability and biocompatibility are critical. Improved erosion resistance in biomedical materials leads to better patient outcomes, lower likelihood of implant failure, and longer device lifespan.
- *Environmental Sustainability:* The study indirectly helps environmental sustainability by addressing erosion issues in industrial and medical settings. Coatings that minimize material loss due to erosion require fewer replacements, reducing resource consumption and waste formation. Enhanced turbine component lifetime in the energy industry promotes more sustainable hydropower operations by reducing the environmental impact of maintenance and downtime.
- *Cross-Disciplinary Collaboration:* The study's investigation into erosion processes and coating performance encourages collaboration across biological and technical fields. This interdisciplinary interchange of information and approaches fosters innovation at the crossroads of materials science, biomechanics, and industrial engineering. It invites academics, engineers, and medical professionals to collaborate on ideas that address common challenges in material durability, performance optimization, and sustainability across various applications.

The coatings analyzed in this study show notable erosion resistance under controlled laboratory slurry conditions. However, it's crucial to evaluate the specific environmental contexts for their practical use. The effectiveness of WC-Co and Cr_3C_2-NiCr coatings may vary depending on the deployment location, such as offshore, in saline conditions, high-humidity areas, or dry inland environments. Consequently, this proposed solution is particularly applicable to hydropower facilities and mechanical systems situated in environments with sediment, turbulence, or

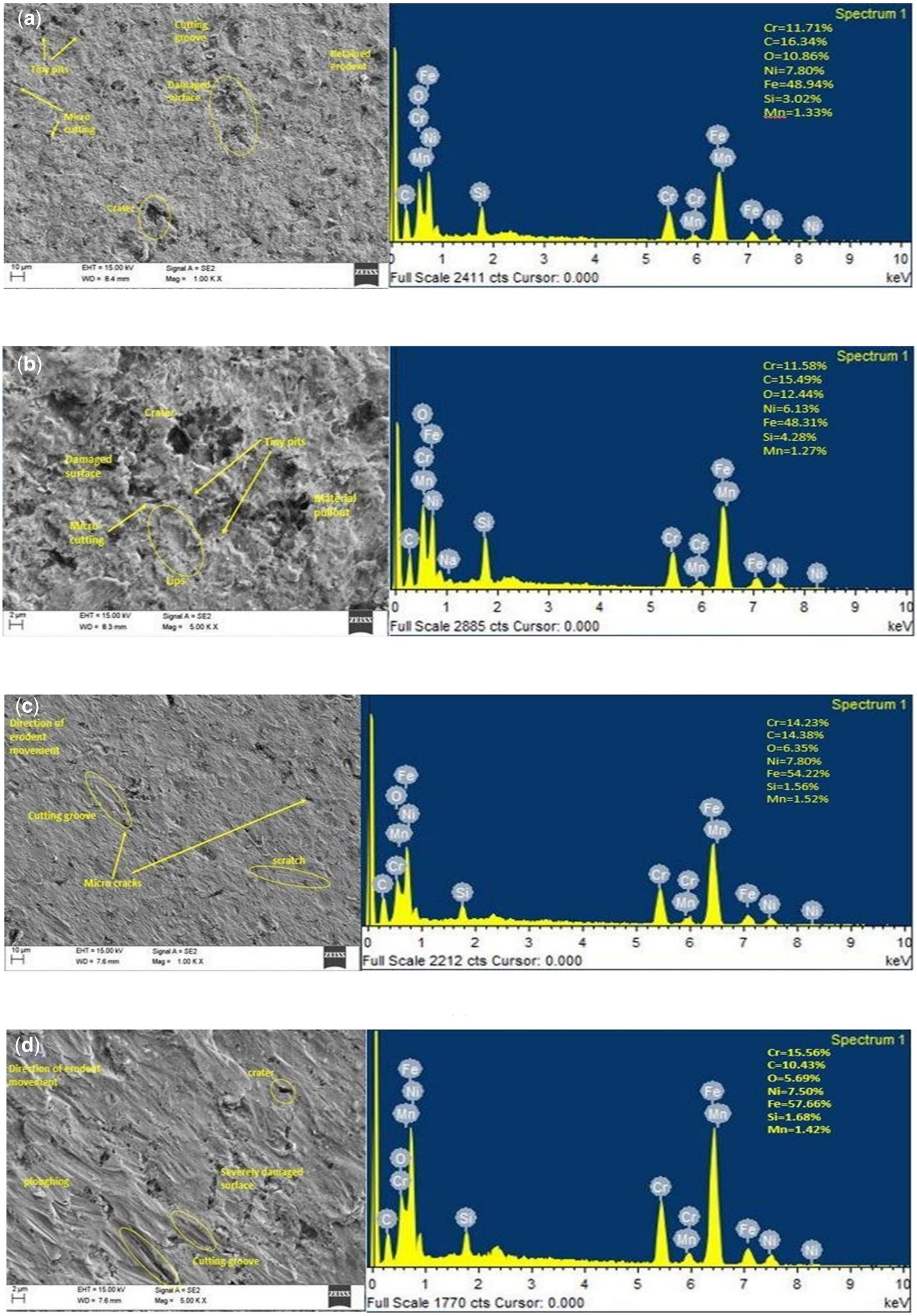

Figure 8. SEM micrographs and EDAX analysis of CF8M-eroded uncoated samples at (a) and (b) 1000× and 5000× magnification and 90° incidence angle, (c) and (d) 1000× and 5000× magnification and 30° incidence angle.

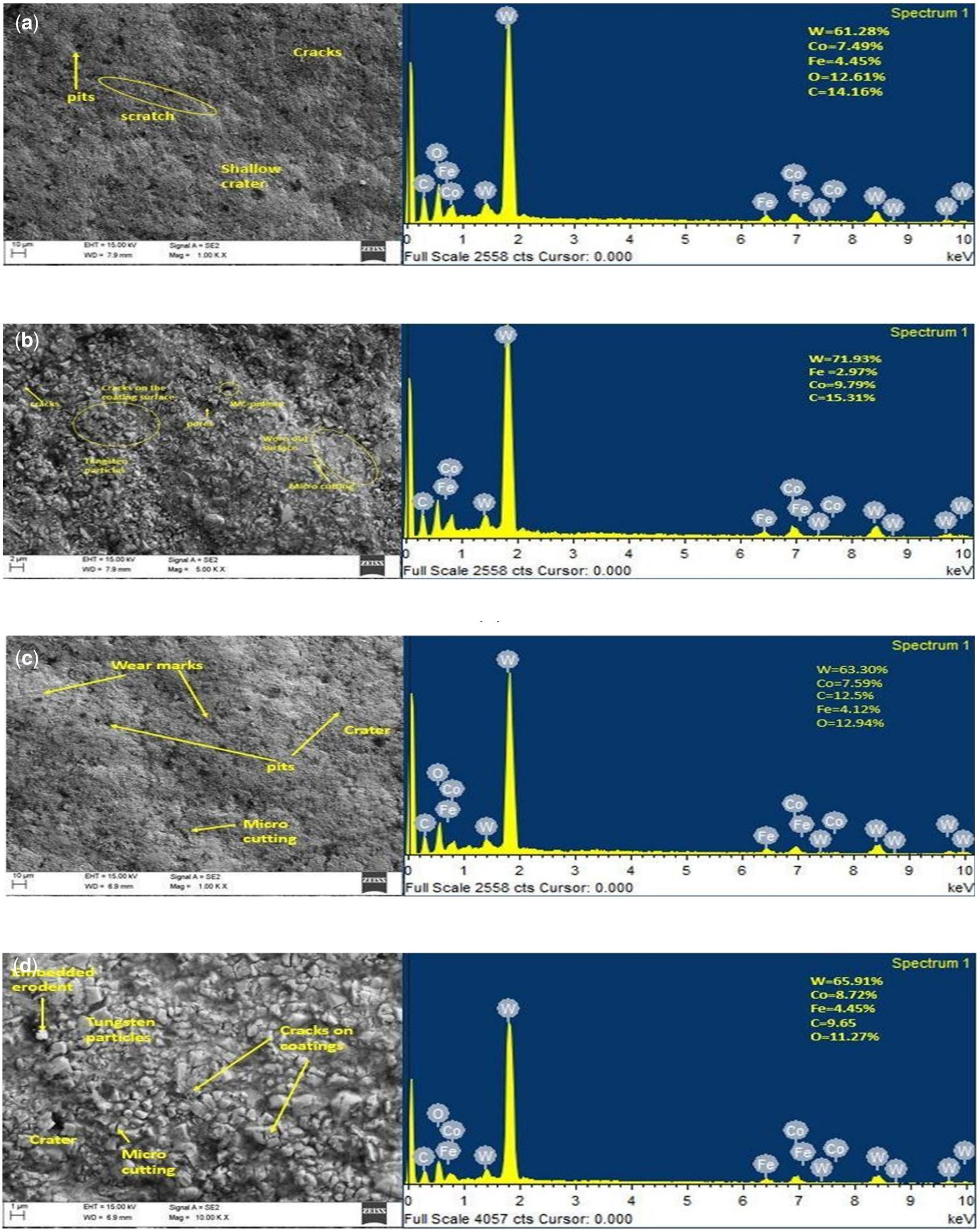

Figure 9. SEM Micrographs and EDAX examination of eroded WC-Co coated samples at (a) and (b) 1000× and 5000× magnification and 90° impingement angle, (c) and (d) 1000× and 5000× magnification and 30° impingement angle.

high moisture levels. Given their proven durability, these coatings can also be reliably utilized in less demanding indoor applications, such as biomedical devices and industrial machinery, where environmental pressures are reduced.

Ultimately, the implications of this study extend beyond technological breakthroughs to encompass economic, environmental, and social benefits. They open the path for future research initiatives, technical advancements, and practical solutions that promote

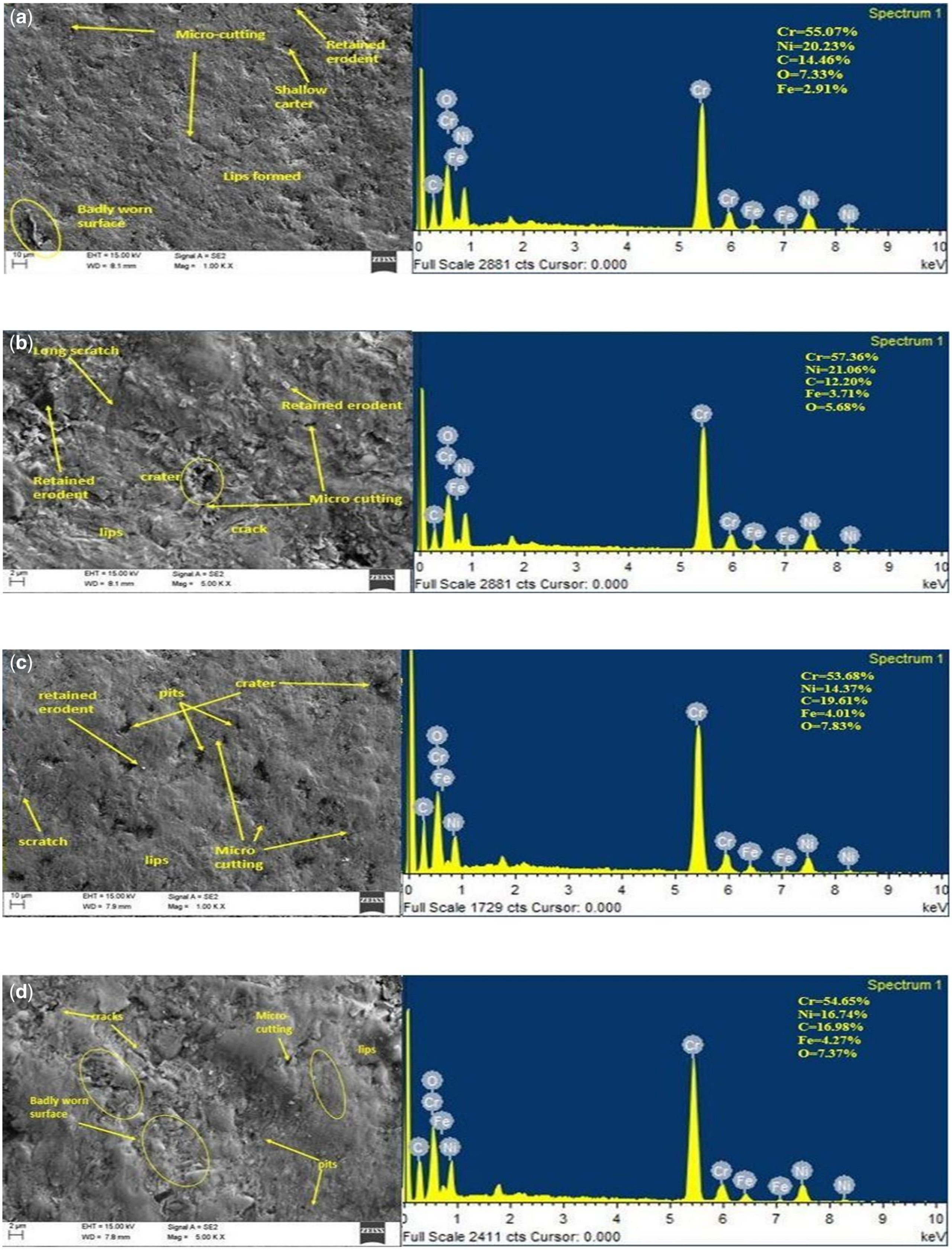

Figure 10. SEM Micrographs and EDAX examination of eroded Cr_3C_2-NiCr coated samples at (a) and (b) 1000× and 5000× magnification and 90˚ impingement angle, (c) and (d) 1000× and 5000× magnification and 30˚ impingement angle.

resilience, efficiency, and sustainability across the biomedical and engineering domains affected by slurry erosion concerns.

Conclusions

Investigating erosion rates in the analyzed specimens leads to various important findings about the parameters that influence erosion behavior and the efficacy of the regression model and optimization.

It is found that the D-gun coatings for WC-Co and Cr_3C_2-NiCr were successfully deposited. It was revealed that WC-Co has superior slurry erosion resistance to uncoated and Cr_3C_2-NiCr. In all testing scenarios, the samples coated with WC show the least material loss. As such, it offered excellent resistance to slurry erosion. Because the material is ductile, the highest erosion for the CF8M substrate occurred at an impingement angle of 30˚. The most significant erosion happened at an impingement angle of 30˚ and a slurry concentration of 20 000 ppm. While WC-Co shows a brittle nature, Cr_3C_2-NiCr demonstrated mixed behavior, meaning it is both brittle and ductile. Even though Cr_3C_2-NiCr is not as resistant to slurry erosion as WC-Co, it is still far superior to uncoated material.

The slurry erosion resistance at both impact angles is reported as follows: uncoated > Cr3C2-NiCr coated > WC-Co coated in decreasing order. Erosion resistance is heavily influenced by the coating material used. WC-Co-coated specimens had low and constant erosion rates, indicating reliable performance. In contrast, CF8M specimens had the greatest mean erosion rate and the most comprehensive variability, indicating a greater vulnerability to erosion. Cr_3C_2-NiCr-coated specimens had moderate erosion rates and moderate variability. These findings underscore the importance of selecting coatings based on their erosion performance to provide practical wear and degradation protection.

Regression analysis demonstrates the effect of slurry concentration and impingement angle on erosion rates. WC-Co-coated specimens show a negative correlation between concentration and angle, implying lower erosion. The ANOVA findings and model summary highlight the strong effects of specimen type, concentration, and angle, with high R-squared values confirming the model's efficacy in explaining erosion variability. The Pareto chart prioritizes essential components that aid in erosion mitigation measures, while residual plots provide feedback for model development. The study identifies material composition, operating parameters, and relationships as essential to erosion resistance. Regression modeling, ANOVA, and graphical analysis provide a thorough knowledge of erosion mechanisms, which aids in developing engineering optimization solutions. These findings contribute to the understanding of erosion mitigation and enhance the selection and design of materials for erosion-prone environments.

The regression findings not only confirm experimental trends but also act as predictive tools applicable in real-world scenarios. They assist in planning maintenance schedules, selecting suitable coatings, and optimizing turbine operations in sediment-rich environments, thereby enhancing performance management and promoting cost-effective lifecycle strategies for hydroelectric turbine systems.

Limitations

While this work provides valuable information about slurry erosion performance and coating efficacy in hydro-turbine steel, certain limitations should be noted. The experimental design may not wholly match real-world operating circumstances, resulting in inconsistencies between laboratory results and field performance. Furthermore, the study focuses on certain coating types and materials, which limits its applicability to a broader variety of coating compositions and application circumstances. Moreover, the study's focus excludes long-term durability assessments and real-time erosion monitoring, critical for assessing coating performance over time and under changing environmental conditions. These constraints underscore the importance of conducting long-term studies that include various coating materials, operational circumstances, and monitoring approaches to fully understand the intricacies of slurry erosion mitigation in actual applications.

Future scope

The future scope of this study encompasses various avenues for further investigation and advancement. Extending the study to encompass various coating materials and compositions may yield valuable insights into the most effective coatings for slurry erosion resistance. Investigating innovative coating methods, such as nanocomposite coatings or surface changes, may improve durability and performance. Furthermore, incorporating real-time monitoring systems and predictive modeling may lead to proactive maintenance measures and a deeper understanding of erosion mechanisms. Exploring innovative materials with inherent erosion-resistant qualities and developing hybrid coatings from various materials may lead to new erosion mitigation opportunities in different industrial settings. Furthermore, considering the influence of environmental elements, such as temperature changes or chemical exposures, on erosion behavior will enhance the study's relevance in real-world scenarios. Overall, the future scope highlights the need for ongoing research and innovation to address the growing challenges in slurry erosion management, while enhancing the reliability and lifespan of engineering components. Although the existing methodology focuses on controlled slurry erosion testing, upcoming experimental frameworks must integrate environmental simulation phases, such as salt spray, humidity, or thermal cycling, to simulate the outdoor and offshore conditions that hydro-turbines encounter in practical applications.

Author contributions

Singh Sukhinderpal (Conceptualization [equal], Investigation [equal], Writing—original draft [equal]), Singh Farwaha Harnam (Data curation [equal], Formal analysis [equal], Resources [equal]), Raman Kumar(Investigation [equal], Methodology [equal], Visualization [equal]), Ariffin I. A (Formal analysis [equal], Methodology [equal], Validation [equal]), N. Beemkumar (Conceptualization [equal], Methodology [equal], Writing—original draft [equal]), Jasmaninder Singh Grewal (Formal analysis [equal], Methodology [equal], Software [equal]), Inderdeep Singh (Formal analysis [equal], Investigation [equal], Visualization [equal]), A. Bhowmik (Data curation [equal], Software [equal], Visualization [equal]), and Wulfran Fendzi Mbasso (Project administration [equal], Supervision [equal], Writing—review & editing [equal])

Conflict of interest: The authors declare that they have no conflict of interest and have no competing interests. All authors have participated in (a) conception and design, or analysis and interpretation of the data; (b) drafting the article or revising it critically for important intellectual content; and (c) approval of the final version.

Funding

This research did not receive any specific grant from funding agencies in the public, commercial, or not-for-profit sectors.

Data availability

Data gathered during research is used in the present work.

References

1. Kumar Goyal D, Singh H, Kumar H, Sahni V. Slurry erosion behaviour of HVOF sprayed WC–10Co–4Cr and Al2O3 + 13TiO2 coatings on a turbine steel. *Wear* 2012;**289**:46–57. https://doi.org/10.1016/j.wear.2012.04.016
2. Pereira Abbade N, João Crnkovic S. Sand–water slurry erosion of API 5L X65 pipe steel as quenched from intercritical temperature. *Tribol Int* 2000;**33**:811–6. https://doi.org/10.1016/S0301-679X(00)00126-2
3. Nouraei H, Wodoslawsky A, Papini M, Spelt JK. Characteristics of abrasive slurry jet micro-machining: a comparison with abrasive air jet micro-machining. *J Mater Process Technol* 2013; **213**:1711–24. https://doi.org/10.1016/j.jmatprotec.2013.03.024
4. Annamalai S, Anand Ronald B, Ebenezer D. The effect of processing techniques and operating parameters on the erosion wear behavior of particle-reinforced metal matrix and surface composites: a review. *J Bio Tribo Corros* 2023;**9**:73.https://doi.org/10.1007/s40735-023-00792-3
5. Kumar Yadav Y, Kumar Singh A, Siddhartha. Insights to improve the tribo-performance of materials used under slurry erosion applications: a review. *Proc Inst Mech Eng Part L J Mat Des Appl* 2023;**237**:3–32. https://doi.org/10.1177/14644207221108565
6. Mayana P, Raviprakash AV, Mohamed Ali S, Mohammed R. Erosion wear behavior of polymer based hybrid composites - a review. *Mater Today Proc* 2023;**77**:424–9. https://doi.org/10.1016/j.matpr.2022.10.263
7. Yan J, Zhou M, Wu H *et al.* A review of key factors affecting the wear performance of medium manganese steels. *Metals* 2023; **13**:1152.https://doi.org/10.3390/met13071152
8. Singla YK, Maughan MR, Arora N, Dwivedi DK. Enhancing the wear resistance of iron-based alloys: a comprehensive review of alloying element effects. *J Manuf Proc* 2024;**120**:135–60. https://doi.org/10.1016/j.jmapro.2024.04.038
9. Tandon D, Li H, Pan Z *et al.* A review on hardfacing, process variables, challenges, and future works. *Metals* 2023;**13**:1512. https://doi.org/10.3390/met13091512
10. Fotovvati B, Namdari N, Dehghanghadikolaei A. On coating techniques for surface protection: a review. *J Manuf Mater Proc* 2019;**3**:28.https://doi.org/10.3390/jmmp3010028
11. Patil RN, Maroor JP, Dhanke JA *et al.* Improving smart agriculture through the use of machine learning to offer tailored crop forecasts. *Remote Sens Earth Syst Sci* 2025;**8**:74–83. https://doi.org/10.1007/s41976-024-00176-2
12. Giurlani W, Berretti E, Innocenti M, Lavacchi A. Measuring the thickness of metal coatings: a review of the methods,". *Coatings* 2020;**10**:1211.https://doi.org/10.3390/coatings10121211
13. Ou YX, Wang HQ, Ouyang X *et al.* Recent advances and strategies for high-performance coatings. *Progr Mater Sci* 2023;**136**: 101125.https://doi.org/10.1016/j.pmatsci.2023.101125
14. Sharma RK, Das RK, Kumar SR. Microstructure, mechanical and tribological properties of high velocity oxy fuel thermal spray coating: a review. *Materialwiss Werkst* 2023;**54**:90–7. https://doi.org/10.1002/mawe.202200101.
15. Snyders R, Hegemann D, Thiry D *et al.* Foundations of plasma enhanced chemical vapor deposition of functional coatings. *Plasma Sources Sci Technol* 2023;**32**:074001.https://doi.org/10.1088/1361-6595/acdabc
16. Babu PS, Madhavi Y, Krishna LR *et al.* Thermal spray coatings for erosion–corrosion resistant applications. *Trans Indian Inst Met* 2020;**73**:2141–59. https://doi.org/10.1007/s12666-020-02053-0
17. Goyal D, Singh H, Kumar H, Sahni V. Erosive wear study of HVOF spray Cr3C2-NiCr coated CA6NM turbine steel. *J Tribol* 2014;**136**:041602.https://doi.org/10.1115/1.4027621
18. Reyes-Mojena MÁ, Sánchez-Orozco M, Carvajal-Fals H *et al.* A comparative study on slurry erosion behavior of HVOF sprayed coatings. *DYNA (Colombia)* 2017;**84**:239–46. https://doi.org/10.15446/dyna.v84n202.56542
19. Sharma V, Kaur M, Bhandari S. Performance investigation of high velocity flame sprayed multi-dimensional Ni-TiO2 and Ni-TiO2-Al2O3 coated hydro turbine steel under slurry erosion. *Wear* 2020;**462-463**:203498.https://doi.org/10.1016/j.wear.2020.203498
20. Kumar R, Bhandari D, Goyal K. Slurry erosion behaviour of HVOF sprayed coatings on hydro turbine steel: a review. In *IOP Conference Series: Materials Science and Engineering,* 2021, vol. 1033, 1 ed. https://doi.org/10.1088/1757-899X/1033/1/012064 [Online]. https://www.scopus.com/inward/record.uri?eid=2-s2.0-85101512286&doi=10.1088%2f1757-899X%2f1033%2f1%2f012064&partnerID=40&md5=48a67b019d298fbec81f7f81cbd6d1df
21. Kumar R, Goyal K, Bhandari D. Slurry erosion behavior of thermally sprayed ceramic nanocomposite coatings on turbine steel. *Int J Applied Ceramic Tech* 2022;**19**:3049–61. https://doi.org/10.1111/ijac.14117
22. Kumar R, Kumar S, Mudgal D. Silt erosion performance of high velocity oxy fuel- (HVOF) sprayed Al2O3–Cr2O3 composite coatings on turbine steel. *Ilt* 2022;**74**:572–9. https://doi.org/10.1108/ILT-08-2021-0346
23. Sahni K, Grewal JS. Slurry erosion behaviour of WC-10Co-4Cr coated CF8M turbine steel. *Mater Today Proceed* 2022;**56**:2666–71. https://doi.org/10.1016/j.matpr.2021.09.236
24. Maekai IA, Harmain GA, Masoodi JH. Resistance to slurry erosion by WC-10Co-4Cr and Cr3C2 – 25(Ni20Cr) coatings deposited by HVOF stainless steel F6NM. *Int J Refrac Metal Hard Mater* 2022;**105**:105830.https://doi.org/10.1016/j.ijrmhm.2022.105830
25. Babu A, Arora HS, Singh RP, Grewal HS. Slurry erosion resistance of microwave derived Ni-SiC composite claddings. *Silicon* 2022;**14**:1069–81. https://doi.org/10.1007/s12633-020-00849-9
26. Paredes RSC, Nikkel W, Sucharski GB, Costa PPB. Optimization of arc-sprayed iron-based tungsten carbide hard coatings on harvester blades. *J Braz Soc Mech Sci Eng* 2019;**41**:217.https://doi.org/10.1007/s40430-019-1719-6
27. Khuengpukheiw R, Saikaew C, Wisitsoraat A. Wear resistance of HVOF sprayed NiSiCrFeB, WC-Co/NiSiCrFeB, WC-Co, and WC-Cr3C2-Ni rice harvesting blades. *Materials Testing* 2021;**63**: 62–72. https://doi.org/10.1515/mt-2020-0009
28. Marques AS, de Costa LDL, dos Santos GR, da Silva Rocha A. Wear study of hot forging punches coated with WC-CoCr and Cr3C2-NiCr through high-velocity oxygen fuel (HVOF) process.

Int J Adv Manuf Technol 2019;**100**:3–11. https://doi.org/10.1007/s00170-018-2693-3
29. Kumar R, Khushdeep G, Bhandari D. Slurry erosion behavior of thermally sprayed nano YSZ reinforced WC-10Co-4Cr ceramic nanocomposite coatings. *Tribol Trans* 2023;**66**:47–58. https://doi.org/10.1080/10402004.2022.2137446
30. Ma X, Ruggerio P. A comparative investigation of feedstock materials on multiple properties of HVOF-formed Cr3C2-NiCr coatings: size effects of powders and carbides on sliding abrasive wear behavior. In *ITSC 2024, Thermal Spray 2024: Proceedings from the International Thermal Spray Conference*, 2024, pp. 558–569. https://doi.org/10.31399/asm.cp.itsc2024p0558
31. Goyal K. Mechanical properties and erosive behaviour of 10TiO2-Cr2O3 coated CA6NM turbine steel under accelerated conditions. *WJE* 2019;**16**:64–70. https://doi.org/10.1108/WJE-08-2018-0262
32. Wolfe DE, Ryan CJ, DeSalle CM *et al.* A comprehensive review of modern engineered ceramics coatings for optimised resistance to wear and corrosion. *Adv Appl Ceram* 2023;**122**:81–100. https://doi.org/10.1080/17436753.2023.2235497
33. Lakkannavar V, Yogesha KB, Prasad CD *et al.* A review on tribological and corrosion behaviour of thermal spray coatings. *J Inst Eng Ser D* 2024. https://doi.org/10.1007/s40033-024-00636-5
34. Nayak SK, Kumar A, Laha T. Fe-based metallic glass coatings by thermal spraying: a focused review on corrosion properties and related degradation mechanisms. *Int Mat Rev* 2023;**68**:404–85. https://doi.org/10.1080/09506608.2022.2084670
35. Sathish M, Radhika N, Saleh B. Duplex and composite coatings: a thematic review on thermal spray techniques and applications. *Met Mater Int* 2023;**29**:1229–97. https://doi.org/10.1007/s12540-022-01302-9
36. Kumar SS, Prasad CD, Hanumanthappa H. Role of thermal spray coatings on erosion, corrosion, and oxidation in various applications: a review. *J Bio Tribo Corros* 2024;**10**. https://doi.org/10.1007/s40735-024-00822-8
37. Ke PL, Wu YN, Sun C. 9 - Detonation gun sprayed thermal barrier coatings. In: Xu H and Guo H (eds), *Thermal Barrier Coatings*. Woodhead Publishing, 2011, 175–89.
38. Kashyap T, Thakur R, Ngo GH *et al.* Silt erosion and cavitation impact on hydraulic turbines performance: An in-depth analysis and preventative strategies. *Heliyon* 2024;**10**:e28998.https://doi.org/10.1016/j.heliyon.2024.e28998
39. Singh H, Kumar R, Prakash C, Singh S. HA-based coating by plasma spray techniques on titanium alloy for orthopedic applications. In: *2nd International Conference on Functional Materials, Manufacturing and Performances, ICFMMP 2021*, vol. 50. Elsevier Ltd, 2021, 612–628. https://doi.org/10.1016/j.matpr.2021.03.165. https://www.scopus.com/inward/record.uri? eid=2-s2.0-85106885193&doi=10.1016%2fj.matpr.2021.03.165&partnerID=40&md5=7830ae340a71c683341e478f34c765fd
40. Lin L, Li G-L, Wang H-D *et al.* Structure and wear behavior of NiCr–Cr3C2 coatings sprayed by supersonic plasma spraying and high velocity oxy-fuel technologies. *Appl Surf Sci* 2015;**356**:383–90. https://doi.org/10.1016/j.apsusc.2015.08.019
41. Ham G-S, Kreethi R, Kim H-J *et al.* Effects of different HVOF thermal sprayed cermet coatings on tensile and fatigue properties of AISI 1045 steel. *J. Mater. Res. Technol* 2021;**15**:6647–58. https://doi.org/10.1016/j.jmrt.2021.11.102
42. Bhandari S, Kansal HK, Singh H *et al.* Slurry erosion testing of detonation gun-sprayed Cr3C2–25NiCr and Cr2O3 coatings on CF8M steel. In: Khangura SS, Singh P, Singh H, Brar GS (eds), *Proceedings of the International Conference on Research and Innovations in Mechanical Engineering*. New Delhi: Springer India, 2014, 415–27.
43. Raj RP, Thirumalaikumarasamy D, Sonar T, Ivanov M. Development of slurry erosion prediction model and studying the effect of slurry erosion parameters on erosion of WC10Ni5Cr coated 35CrMo steel. *Int J Interact Des Manuf* 2025;**19**:219–38. https://doi.org/10.1007/s12008-023-01619-8
44. Javaheri V, Porter D, Kuokkala V-T. Slurry erosion of steel—review of tests, mechanisms and materials. *Wear* 2018;**408-409**:248–73. https://doi.org/10.1016/j.wear.2018.05.010
45. Anderson K, Karimi S, Shirazi S. Erosion testing and modeling of several non-metallic materials. *Wear* 2021;**477**:203811.https://doi.org/10.1016/j.wear.2021.203811
46. Polyakov V, Baffaut C, Ferro V, Van Pelt S. Advances in soil erosion research: mechanisms, modeling and applications—a special issue in honor of Dr Mark Nearing. *Int Soil Water Conserv Res* 2023;**11**:589–91. https://doi.org/10.1016/j.iswcr.2023.08.006
47. Kumar R, Rafighi M, Özdemir M *et al.* Modeling and optimization of hard turning: predictive analysis of surface roughness and cutting forces in AISI 52100 steel using machine learning. *Int J Interact Des Manuf* 2024. https://doi.org/10.1007/s12008-024-02166-6
48. Karim MR, Kumar R, Babbar A *et al.* Surface roughness and cutting force in turning of alkaline-treated banana fibre-reinforced polymer composite: compressed air cutting. *J Reinforced Plastics and Compos* 2024;07316844241228935, in press. https://doi.org/10.1177/07316844241228935
49. Sidhu AS, Kumar R, Singh S, Kaur H. "Efficiency enhancement and energy optimization in alloy steel drilling: an experimental and statistical analysis," in *Intelligent Manufacturing and Energy Sustainability*, Singapore, P. H. V. S. Talpa Sai, S. Potnuru, M. Avcar, and V. Ranjan Kar, Eds., 2024//2024: Springer Nature Singapore, pp. 269–79.
50. Kumar R, Bilga PS, Singh S. An investigation of energy efficiency in finish turning of en 353 alloy steel. In: Sangwan KS, Herrmann C (eds), *28th CIRP Conference on Life Cycle Engineering, LCE 2021*, vol. 98, Elsevier B.V, 2021, 654–9. https://doi.org/10.1016/j.procir.2021.01.170. https://www.scopus.com/inward/record.uri? eid=2-s2.0-85102615331&doi=10.1016%2fj.procir.2021.01.170&partnerID=40&md5=a7fdc09e27f03e2ff35ba0b212714529
51. Channi AS, Bains HS, Grewal JS *et al.* Exploring the application sphere of electrical discharge machining in composite materials considering surface features: a content analysis. *Int J Interact Des Manuf* 2023;**17**:2095–114. https://doi.org/10.1007/s12008-022-01060-3
52. Kumar R, Singh S, Aggarwal V *et al.* Hand and abrasive flow polished tungsten carbide die: optimization of surface roughness, polishing time and comparative analysis in wire drawing. *Materials* 2022;**15**:1287. https://doi.org/10.3390/ma15041287
53. Kumar R, Channi AS, Kaur R *et al.* Exploring the intricacies of machine learning-based optimization of electric discharge machining on squeeze cast TiB2/AA6061 composites: insights from morphological, and microstructural aspects in the surface structure analysis of recast layer formation and worn-out analysis. *J. Mater. Res. Technol* 2023;**26**:8569–603. https://doi.org/10.1016/j.jmrt.2023.09.127
54. Goyal KK, Sharma N, Dev Gupta R *et al.* A soft computing-based analysis of cutting rate and recast layer thickness for AZ31 alloy on WEDM using RSM-MOPSO. *Materials* 2022;**15**:635.https://doi.org/10.3390/ma15020635
55. Peat T, Galloway A, Toumpis A *et al.* Performance evaluation of HVOF deposited cermet coatings under dry and slurry erosion.

Surf Coat Technol 2016;**300**:118–27. https://doi.org/10.1016/j.surfcoat.2016.05.039
56. Anpo M, Costentin G, Giamello E *et al.* Characterisation and reactivity of oxygen species at the surface of metal oxides. *J Catalys* 2021;**393**:259–80. https://doi.org/10.1016/j.jcat.2020.10.011
57. Alroy RJ, Kamaraj M, Lakshmi DV *et al.* Tailoring microstructural features of Cr3C2-25NiCr coatings through diverse spray variants and understanding the high-temperature erosion behavior. *Tribol Int* 2023;**188**:108810.https://doi.org/10.1016/j.triboint.2023.108810
58. Matthews S. Development of high carbide dissolution/low carbon loss Cr3C2–NiCr coatings by shrouded plasma spraying. *Surf Coat Technol* 2014;**258**:886–900. https://doi.org/10.1016/j.surfcoat.2014.07.062

Oxford Open Materials Science, 2025, 5, 1–23
https://doi.org/10.1093/oxfmat/itaf008
Research article